Development of motor neurons and motor activity in zebrafish requires F-actin nucleation by Fmn2b

Dhriti Nagar[1], Blake Carrington[2], Shawn M Burgess[3] and Aurnab Ghose[1*]

[1] Indian Institute of Science Education and Research (IISER) Pune, Dr Homi Bhabha Road, Pune 411008, INDIA

[2] Zebrafish Core, Translational and Functional Genomics Branch, National Human Genome Research Institute, National Institutes of Health, Bethesda, Maryland, USA

[3] Translational and Functional Genomics Branch, National Human Genome Research Institute (NHGRI), National Institutes of Health (NIH), Bethesda, MD, USA

* Correspondence: Dr. Aurnab Ghose, Indian Institute of Science Education and Research (IISER) Pune, Dr Homi Bhabha Road, Pune 411008, INDIA.

Email: aurnab@iiserpune.ac.in

ABSTRACT

Background

Cytoskeletal remodelling plays a pivotal role in the establishment of neuronal connectivity during development and in plasticity in adults. Mutations in the cytoskeleton regulatory protein Formin-2 (Fmn2) are associated with neurodevelopmental disorders like intellectual disability, though its function in neuronal morphogenesis has not been characterised *in vivo*.

Results

Here we develop a loss-of-function model for *fmn2b*, the zebrafish orthologue of Fmn2, using CRISPR/Cas9-mediated gene editing. *fmn2b* mutants display motor deficits starting from the earliest motor responses in the embryo. We find that *fmn2b* is expressed in motor neurons and its loss reduces motor neuron innervation of the axial muscles without affecting myotome integrity. The translocation of caudal primary (CaP) motor neuron outgrowth is compromised in *fmn2b* mutants, while rostral primary (RoP) motor neurons have missing soma or stall at the horizontal myoseptum. Strikingly, axon collateral branching of the motor neurons is severely compromised and results in reduced synaptic coverage of the myotome. Rescue experiments identify the requirement for Fmn2-mediated actin nucleation for motor neuron outgrowth and arborisation.

Conclusions

The zebrafish loss-of-function model of Fmn2 reveals the specific requirement of F-actin polymerisation by Fmn2 in neuromuscular development. It also underscores the role of Fmn2 in motor neuropathies, especially as a proportion of individuals harbouring mutations in Fmn2 present with hypotonia.

43 **Keywords**

44 Fmn2b, motor behaviour, motor neurons, axonal branching, actin nucleation

45 **INTRODUCTION**

46 Developing neurons migrate to their predetermined targets, undergo axonogenesis,
47 pathfinding and eventually arborize to make functional synapses. Cytoskeletal
48 remodelling allows dynamic interactions of the developing neurons with the
49 environment during outgrowth, pathfinding and arborization (Dickson, 2002; Lowery
50 and Van Vactor, 2009; Gordon-Weeks and Fournier, 2014; Flynn and Bradke, 2020)
51 aided by several actin remodelling proteins (Dent et al., 2011; Kessels et al., 2011;
52 Lewis et al., 2013; Coles and Bradke, 2015; Armijo-Weingart and Gallo, 2017).

53 Remodelling of actin filaments allows protrusive structures to probe the environment
54 for cues in the form of growth cone filopodia and axonal and dendritic branches
55 (Lowery and Van Vactor, 2009; Lewis et al., 2013; Armijo-Weingart and Gallo, 2017;
56 Menon and Gupton, 2018).

57 In zebrafish, motor neurons exit perpendicular to the spinal cord and traverse the
58 myotomes to arborize and make synapses onto the axial muscles (Myers et al., 1986;
59 Westerfield et al., 1986). Adequate innervation of muscles by the motor neurons is
60 ensured by hemisegment specific outgrowth, pathfinding and arborization. Precise
61 neuronal morphogenesis of motor neurons is critical for achieving context-specific
62 synaptic drive at the level of muscles, enabling the organism to execute motor
63 behaviours.

64 Actin nucleating proteins are a major class of actin remodelling factors and have been
65 implicated in neuronal morphogenesis. The actin nucleator Cobl localizes to regions
66 with high actin dynamics and is implicated in the maintenance of neurite branching
67 (Ahuja et al., 2007). Actin nucleators mediate the local rearrangement of actin
68 filaments via the formation of dynamic structures like F-actin patches and F-actin blobs

and regulate the initiation of protrusions and branching (Ketschek and Gallo, 2010; Spillane et al., 2011; Spillane and Gallo, 2014; Nithianandam and Chien, 2018; Kundu et al., 2020). Reports have characterized the role of Dishevelled associated activator of morphogenesis (Daam) formins in *Drosophila* axonal growth (Matusek et al., 2008; Prokop et al., 2011) and Daam1a in habenular morphogenesis and IPN connectivity in zebrafish (Colombo et al., 2013). Another study identified Formin-3 (Form3) in the maintenance of complex dendritic arbours of nociceptive sensory neurons in *Drosophila* via microtubule stabilization and adequate organelle trafficking (Das et al., 2021). However, the function of formin family of actin nucleators in axonal branching *in vivo* remains elusive.

Formin-2 (Fmn2) is part of the FMN family of formins and is known to be involved in neuronal development. Biallelic mutations in Fmn2 cause neurodevelopmental defects resulting in intellectual disability and muscle hypotonia in humans (Law et al., 2014). Primary hippocampal neurons from Fmn2 null mice show defective dendritic spine morphogenesis (Law et al., 2014) and there is increasing evidence implicating copy number variations (CNVs) and single nucleotide polymorphisms (SNPs) in Fmn2 in sporadic Amyotrophic Lateral Sclerosis (SALS) (Schymick et al., 2007; Pamphlett et al., 2011; Morello et al., 2018). Fmn2 has previously been characterized in outgrowth, pathfinding (Sahasrabudhe et al., 2016; Ghate et al., 2020; Kundu et al., 2021) and axonal branching (Kundu et al., 2020) in chick spinal primary neurons *in vitro*. Depletion of Fmn2 causes reduced growth cone motility and mechanotransduction in chick spinal primary neurons (Sahasrabudhe et al., 2016; Ghate et al., 2020). Fmn2 regulates the stabilization of actin patches required for the initiation of axonal branching in cultured chick spinal neurons by insulating the actin patch from actin depolymerizing factors like ADF (Kundu et al., 2020). Morpholino-mediated transient

knockdown of Fmn2b, the zebrafish ortholog of Fmn2, causes impaired outgrowth of the spiral fiber neuron commissures in the hindbrain and results in diminished short latency escape response (Nagar et al., 2021).

In this study, we generate *fmn2b* mutants using the CRISPR-Cas9 based gene editing to assess the contribution of Fmn2b in neural circuit development and behaviour and to improve our understanding of the mechanistic underpinnings of the neurodevelopmental disorders associated with Fmn2.

Motor neurons are the final, executory neurons driving motor responses. In zebrafish, the motor neurons receive synaptic inputs from reticulospinal neurons, including the Mauthner cell and several hindbrain interneurons, which regulate motor neuron function in response to stimuli (Bernhardt et al., 1990; Hale et al., 2001; McLean and Fetcho, 2008). Three subtypes of primary motor neurons are present on either side of the spinal cord – the Caudal primary (CaP), the Middle primary (MiP) and the Rostral primary (RoP) – with distinct morphology and muscle targets (Eisen et al., 1986; Myers et al., 1986; Bernhardt et al., 1990; Melançon et al., 1997; Stifani, 2014). The myotomes are also innervated by secondary motor neurons which develop after the primary motor neurons and have less complex arborization fields (Pike et al., 1992; Beattie et al., 1997; Menelaou and Svoboda, 2009). Motor neurons innervate the target muscles to form structurally and functionally distinct motor units and regulate the overall synaptic drive of the muscles during motor behaviours (Saint-Amant and Drapeau, 1998; Drapeau et al., 2002; Bagnall and McLean, 2014; Bello-Rojas et al., 2019).

116 This study uncovers the role of the zebrafish orthologue of Formin-2, Fmn2b, in
117 regulating motor neuron outgrowth and branching *in vivo* and the consequent effects
118 on motor behaviour.

119 # RESULTS

120 ### *Generating fmn2b CRISPR mutants*

121 Zebrafish has two paralogs of Formin-2, *fmn2a* and *fmn2b*. *fmn2b*, located on
122 chromosome 12, has higher sequence homology with human Fmn2 compared to
123 *fmn2a* and has the characteristic Formin Homology 1 (FH1), Formin Homology 2 (FH2)
124 and Formin Spire Interaction (FSI) domains (Nagar et al., 2021). In contrast, the FH1
125 domain of *fmn2a* is truncated. As observed in humans, rodents and chicks (Leader
126 and Leder, 2000; Sahasrabudhe et al., 2016), *fmn2b* mRNA is enriched in the
127 zebrafish nervous system whereas *fmn2a* shows no detectable expression in the
128 nervous system of zebrafish (Nagar et al., 2021). In this study, we used the CRISPR-
129 Cas9 technology to generate mutants of *fmn2b*, the functional ortholog of mammalian
130 Fmn2 in zebrafish.

131 To generate *fmn2b* knockout zebrafish, sgRNAs targeting the exon 1 of *fmn2b* were
132 designed using the CRISPRscan tool (Moreno-Mateos et al., 2015) and cross verified
133 for high scores using the ZebrafishGenomics track (LaFave et al., 2014) in UCSC
134 genome browser. Exon 1 was targeted to ensure that the resulting mutant would lack
135 the functional domains.

136 The embryos injected with sgRNA and Cas9 mRNA were raised till sexual maturity.
137 Individual embryos from the injected clutch were outcrossed with wildtype fish of the
138 opposite sex to obtain eggs that were genotyped using fluorescent PCR (Varshney et
139 al., 2016). Multiple founder lines with different allelic mutations were identified for
140 *fmn2b* by fluorescent-PCR. The F1 progeny obtained from the outcross of these
141 founder lines was raised to adulthood and the siblings were in-crossed. The F2
142 progeny were raised to adulthood and genotyped using the caudal fin clip method and

143 subsequent Sanger sequencing of the genomic locus flanking the sgRNA-1 target
144 sequence to determine whether they were heterozygous or homozygous for the
145 inherited mutant allele.

146 The sgRNA caused various indels near the intended target around 696 bp into the
147 *fmn2b* cDNA sequence in exon 1, corresponding to 232nd amino acid position in the
148 1454 amino acid long Fmn2b protein sequence. Two alleles causing a 7 bp
149 (*fmn2b*$^{\Delta 7/\Delta 7}$) and a 4 bp (*fmn2b*$^{\Delta 4/\Delta 4}$) deletion, respectively, were selected and
150 maintained as homozygous mutants (Figure 1 A-B). The deletions result in premature
151 stop codons at the 280th or the 281st amino acid in the *fmn2b*$^{\Delta 7/\Delta 7}$and *fmn2b*$^{\Delta 4/\Delta 4}$
152 mutants, respectively (Figure 1 C). The two homozygous mutant alleles were in-
153 crossed to obtain heteroallelic *fmn2b* mutants (*fmn2b*$^{\Delta 4/\Delta 7}$) and used in subsequent
154 experiments.

155 ***fmn2b mutants exhibit Spontaneous Tail Coiling (STC) and Touch-Evoked***
156 ***Escape Response (TEER) deficits***

157 The first motor behaviour to appear in the developing zebrafish embryo is spontaneous
158 tail coiling (STC) which starts around 17 hpf and persists till 27 hpf (Saint-Amant and
159 Drapeau, 1998; Brustein et al., 2003). We recorded the spontaneous tail coiling in
160 *fmn2b*$^{+/+}$ and *fmn2b*$^{\Delta 4/\Delta 7}$ embryos at 22 hpf (Movie 1). The frequency of spontaneous
161 tail coiling was reduced in *fmn2b*$^{\Delta 4/\Delta 7}$ mutant embryos (3.168 ± 0.314 min^{-1}) as
162 compared to the wild-type *fmn2b*$^{+/+}$ embryos (5.003 ± 0.203 min^{-1}) (Figure 2 A).
163 However, the maximum amplitude of tail coiling did not change significantly in the
164 *fmn2b*$^{\Delta 4/\Delta 7}$ embryos (Figure 2 B). The decrease of coiling frequency but not the
165 magnitude of coiling indicates that the defects are likely due to deficits in the motor
166 neuron or the neuromuscular junction (NMJ) function rather than loss of muscle
167 integrity.

168 As the embryo develops, the motor circuits mature to mediate touch-evoked escape
169 responses (TEER) beginning at 48 hpf. TEER is typically manifested as a fast C-bend
170 escape followed by a swimming bout. We performed the TEER assay on *fmn2b*$^{+/+}$ and
171 *fmn2b*$^{\Delta 4/\Delta 7}$ embryos at 60 hpf (Movie 2) and recorded their response at 200 fps. Both
172 the distance traversed (13.55 ± 1.06 mm) and the average speed (34.26 ± 2.785 mm/s)
173 of touch-evoked swimming was reduced in 60 hpf *fmn2b*$^{\Delta 4/\Delta 7}$ embryos as compared
174 to the distance covered (65.31 ± 4.93 mm) and swim speed (84.37 ± 3.253) of *fmn2b*$^{+/+}$
175 embryos (Figure 2 C, D, E). However, the maximum instantaneous speed attained
176 during the entire swim bout was not significantly different between *fmn2b*$^{+/+}$ (199.5 ±
177 7.039 mm/s) and *fmn2b*$^{\Delta 4/\Delta 7}$ embryos (183.2 ± 6.245 mm/s) (Figure 2 F).

178 The comparable maximum tail coiling amplitudes and maximum instantaneous speeds
179 observed in *fmn2b*$^{+/+}$ and *fmn2b*$^{\Delta 4/\Delta 7}$ embryos suggest abnormal motor neuron
180 development or NMJ function and is unlikely to involve deficits in the musculature.
181 Consistent with this, phalloidin staining of the *fmn2b*$^{\Delta 4/\Delta 7}$ embryos revealed no
182 structural deformities in the axial muscles compared to the *fmn2b*$^{+/+}$ embryos (Figure
183 S1).

184 ***fmn2b mRNA is expressed in the spinal cord and motor neurons of zebrafish***
185 ***embryos***

186 The time window of STC and TEER in zebrafish embryos coincides with the outgrowth
187 and pathfinding of primary motor neurons (Myers et al., 1986). *fmn2b* mRNA was
188 found to be expressed in the spinal cord 48 hpf onwards suggesting a possible role in
189 the development of spinal neurons (Figure 3 A, B). Previous reports have also reported
190 Fmn2 mRNA expression in the spinal cord of chick, mouse and human embryos
191 (Leader and Leder, 2000; Sahasrabudhe et al., 2016). To explicitly test the expression
192 of *fmn2b* mRNA in the motor neurons, GFP positive motor neurons were isolated using

193 Fluorescence-activated cell sorting (FACS) from 24 hpf and 60 hpf *Tg(mnx1:GFP)*
194 embryos and the expression of *fmn2b* evaluated by RT-PCR. *fmn2b* transcript was
195 expressed in motor neurons expressing GFP driven by the Tg(mnx1:GFP) isolated
196 from both 24 hpf and 60 hpf embryos (Figure 3 C). Therefore, *fmn2b* is expressed in
197 the spinal cord and in the motor neurons of zebrafish embryos and could mediate
198 motor neuron development and function.

199 ***CaP motor neuron outgrowth is slower in fmn2b mutants***

200 To test the hypothesis that the motor defects in *fmn2b* mutants may arise due to
201 deficits in motor neuron morphogenesis, the *fmn2b*$^{\Delta 4/\Delta 7}$ mutant line was crossed with
202 the *Tg(mnx1:GFP)* line to obtain homozygous *fmn2b* mutants in the transgenic
203 background of GFP-labelled motor neurons. The development of motor neurons was
204 observed from 22 hpf to 26 hpf using time-lapse confocal imaging of the GFP-labelled
205 neurons (Movie 3). The growth cones of the pioneering caudal primary (CaP) motor
206 neurons were tracked using the Manual Tracking plugin in ImageJ, and the average
207 translocation speed was calculated. The *fmn2b*$^{\Delta 4/\Delta 7}$ embryos showed slow outgrowth
208 of the CaP neurons (Figure 3 D, E). The growth cone translocation speed of *fmn2b*$^{\Delta 4/\Delta 7}$
209 embryos (22.1 ± 1.575 μm/h) was slower than the *fmn2b*$^{+/+}$ embryos (28.34 ± 1.962
210 μm/h) (Figure 3 F).

211 ***Primary motor neuron outgrowth and branching defects in fmn2b mutants***

212 In addition to the slow outgrowth of CaP motor neurons in *fmn2b* mutants, collateral
213 branches extended by the motor neurons at 24 hpf (Figure 4 A, B) and 60 hpf (Figure
214 4 G, H) were observed using the *fmn2b* mutant line *fmn2b*$^{\Delta 4/\Delta 7}$ in the background of
215 the transgenic line *Tg(mnx1:GFP).* The embryos were mounted laterally to image the
216 motor neurons and the images traced and quantified using the NeuronJ plugin in

217 ImageJ. At 24 hpf, 100% of the hemisegments had the CaP motor neuron soma
218 present in *fmn2b*$^{+/+}$ as well *fmn2b*$^{\Delta 4/\Delta 7}$ embryos. The branch density along the fascicle
219 length (Figure 4 E) and the length of the motor fascicle (Figure 4 F) extended by the
220 primary motor neurons at 24 hpf was found to be reduced in *fmn2b*$^{\Delta 4/\Delta 7}$ embryos.
221 Similarly, 60 hpf *fmn2b*$^{\Delta 4/\Delta 7}$ embryos showed a reduction in the density (Figure 4 K) of
222 collateral branches along the motor fascicle along with a reduction in the fascicle
223 length (Figure 4 L).

224 These observations implicate *fmn2b* function in both the outgrowth of the CaP motor
225 neuron and collateral branching of motor neurons.

226 ***F-actin nucleation activity of Fmn2 is required for motor neuron branching***

227 The functional domains characteristic of Formin-2 are conserved across vertebrates
228 and ectopic expression of full-length mouse Fmn2 (mFmn2) can rescue
229 neurodevelopmental defects induced by morpholino-mediated knockdown of Fmn2b
230 in zebrafish (Nagar et al., 2021). To assess if the expression of exogenous Fmn2 could
231 rescue the outgrowth and branching defects, *mFmn2* mRNA tagged with mCherry was
232 injected in the *fmn2b*$^{\Delta 4/\Delta 7}$ mutant embryos at the 1-cell stage. The branch density and
233 fascicle length defects were rescued in both 24 hpf (Figure 4 C, E, F) and 60 hpf
234 (Figure 4 I, K, L) mutant embryos.

235 F-actin nucleation is the canonical function of formins, including Fmn2, and is
236 mediated by the FH2 domain (Goode and Eck, 2007; Quinlan et al., 2007; Yoo et al.,
237 2015). The FH2 domain is conserved across phyla, including zebrafish (Nagar et al.,
238 2021). A conserved isoleucine residue (at position 1226 in mouse Fmn2) is known to
239 be critical for actin nucleation (Quinlan et al., 2007; Roth-Johnson et al., 2014; Kundu
240 et al., 2020). Clustal omega alignment of the conserved isoleucine residue is shown

241 in Figure S2. To test if actin nucleation by Fmn2b is required in zebrafish motor neuron
242 morphogenesis, an F-actin nucleation dead version of mFmn2 with a point mutation
243 converting the Isoleucine at 1226 amino acid position to Alanine (mFmn2-I1226A) was
244 used. The mRNA for mFmn2-I1226A tagged with mCherry was injected in the
245 *fmn2b*$^{\Delta 4/\Delta 7}$ embryos at the 1-cell stage and the motor neuron development was
246 analyzed.

247 The *mFmn2-I1226A* mRNA injected 24 hpf (Figure 4 D, E, F) and 60 hpf (Figure 4 J,
248 K, L) mutant embryos continue to exhibit the outgrowth and branching defects similar
249 to the *fmn2b*$^{\Delta 4/\Delta 7}$ embryos. Rescue of phenotype exhibited by the *fmn2b*$^{\Delta 4/\Delta 7}$ mutants
250 by full-length mFmn2 but not the nucleation dead version, mFmn2-I1226A points
251 towards the conserved function of Fmn2 in motor neuron development and highlights
252 the significance of F-actin nucleation by Fmn2 in outgrowth and branching of motor
253 neurons.

254 ***Rostral Primary (RoP) motor neuron development is compromised in fmn2b***
255 ***mutants***

256 Despite slower outgrowth rates and reduced branching in *fmn2b*$^{\Delta 4/\Delta 7}$ embryos, the
257 CaP fascicle eventually reaches the extremity of the ventral musculature in the
258 zebrafish flank. On the contrary, another class of primary motor neurons, the Rostral
259 primary (RoP) motor neurons which typically project to the mid-dorsal and mid-ventral
260 musculature (Bagnall and McLean, 2014; Bello-Rojas et al., 2019), are permanently
261 affected in *fmn2b*$^{\Delta 4/\Delta 7}$ embryos. The RoP soma are located at their predetermined site
262 adjacent to the CaP and VaP cell body cluster in the spinal cord. The cell bodies of
263 primary motor neurons are distinctly recognizable at 24 hpf.

264 On examining the 24 hpf embryos, the RoP cell body was found to be missing in *fmn2b*
265 mutants. Compared to 2.5% of the hemisegments in *fmn2b*$^{+/+}$ embryos, 46.87% of the
266 hemisegments in *fmn2b*$^{\Delta 4/\Delta 7}$ embryos did not have the RoP cell body. Injection of 1-
267 cell stage *fmn2b*$^{\Delta 4/\Delta 7}$ embryos with *mFmn2* mRNA rescued this defect with only 2.85%
268 hemisegments lacking RoP soma. However, the actin nucleation dead *mFmn2-I1226A*
269 mRNA failed to rescue the loss of RoP soma in *fmn2b* mutants and 43.75% of the
270 hemisegments continued to show loss of RoP soma (Figure 5 A-F).

271 At 60 hpf, the RoP motor neurons innervate their target in the mid-dorsal and mid-
272 ventral musculature. The RoP motor neurons in *fmn2b*$^{\Delta 4/\Delta 7}$ mutants showed two major
273 types of defects, absence of RoP outgrowth and stalling of RoP at the choice point
274 near the horizontal myoseptum (HMS), where the RoP axons take a sharp lateral turn.

275 In the *fmn2b* mutant embryos, 91.3% of the hemisegments analyzed showed little to
276 no lateral innervation. Of these, 44.35% of the hemisegments displayed defasciculated
277 axons near the horizontal myoseptum, which acts as a choice point for the RoP axons
278 to turn laterally. The hemisegments with defasciculated axons were classified as
279 stalled RoP axons. Similar defects in RoP-like secondary motor neurons have been
280 reported to occur due to depletion of Kif1b and Fidgetin like-1 in zebrafish (Fassier et
281 al., 2018; Atkins et al., 2019). However, 46.95% of hemisegments had no RoP
282 innervation altogether and were classified as RoP absent. Only 8.7% hemisegments
283 showed the stereotypical RoP innervation and were classified as RoP present. In the
284 *fmn2b*$^{+/+}$ embryos, only 3.15% of the hemisegments quantified showed RoP stalling
285 defects, and the rest had stereotypical innervation by the RoP neurons. The RoP
286 stalling and outgrowth defects were rescued by injection of full-length *mFmn2* mRNA
287 with only 10.16% hemisegments with RoP stalling and 8.47% hemisegments with RoP
288 outgrowth defects. On the other hand, RoP defects persisted in the *fmn2b*$^{\Delta 4/\Delta 7}$

289 embryos injected with *mFmn2-I1226A* mRNA, with 18.3% of hemisegments having
290 stalled RoP axons and 81.7% without RoP innervation (Figure 5 G-L).

291 Collectively, these results indicate that *fmn2b* has pleiotropic effects on RoP
292 development dependent on F-actin nucleation function. The deficits are at the level of
293 loss of RoP soma, deficits in RoP axonogenesis and stalling at the horizontal
294 myoseptum choice point.

295 ***Effect of overexpression of Fmn2 in motor neurons***

296 The role of *fmn2b* in motor neuron development has been established so far by
297 observing *fmn2b* mutants, where the loss of Fmn2b in motor neurons causes a
298 reduction in outgrowth and branching. Overexpression of mouse Fmn2 was employed
299 in wildtype embryos to test the phenotypes in the context of Fmn2 gain of function.
300 The embryos overexpressing mFmn2 showed increased branching, but
301 overexpression of the nucleation dead mFmn2-I1226A did not cause any significant
302 changes and was comparable to the wild-type embryos (Figure 6 A, B, E, F). The
303 branch density was found to be increased in mFmn2 mRNA injected embryos at 24
304 hpf as well as 60 hpf but not in mFmn2-I1226A mRNA injected group (Figure 6 C, G).
305 Interestingly, in 24 hpf embryos, the fascicle length was not significantly different in
306 embryos overexpressing mFmn2 but was found to be decreased in embryos
307 overexpressing mFmn2-I1226A. In 60 hpf embryos, the fascicle length was slightly
308 increased in the mFmn2 overexpression group but remain unaffected in the mFmn2-
309 I1226A overexpression group (Figure 6 D, H).

310 However, quantification of RoP soma and RoP axon outgrowth phenotypes in the
311 *fmn2b*$^{+/+}$ embryos overexpressing mFmn2 and mFmn2-I1226A did not reveal any
312 significant changes (Figure S3).

313 ***Neuromuscular Junction (NMJ) development in fmn2b mutants***

314 Primary motor neurons innervate the fast-twitch muscles and form functional synapses
315 by 48 hpf. To visualize the neuromuscular junctions (NMJ), double immunostaining of
316 whole-mount 60 hpf embryos with znp-1 antibody (presynaptic marker) and α-
317 bungarotoxin (post-synaptic marker) were undertaken. The co-localization of the pre-
318 and post-synaptic markers revealed the engaged NMJ synapses in *fmn2b*$^{+/+}$ and
319 *fmn2b*$^{\Delta 4/\Delta 7}$ embryos (Figure 7 A, B). Synapses (co-localization of znp-1 and α-
320 bungarotoxin signals) along the neuronal arbours were quantified using the
321 SynapCountJ plugin in Fiji. The number of synapses identified was normalized to the
322 area of the myotome corresponding to one somite and the length of the neuronal
323 arbour.

324 The *fmn2b*$^{\Delta 4/\Delta 7}$ mutants show reduced synaptic coverage of the myotomes compared
325 to *fmn2b*$^{+/+}$ embryos (Figure 7 C). This result is consistent with previous observations
326 of reduced outgrowth and branching density, and therefore the attenuated occupancy
327 of myotome area, of motor neurons.

328 However, the number of synapses normalized to the arbour length was found to be
329 comparable (Figure 7 D). Thus, while the ability of motor neurons to form synapses is
330 intact in *fmn2b* mutants, the dramatically reduced arborization results in an effective
331 reduction in the total number of synapses per myotome. The locomotor defects
332 observed in *fmn2b* mutants is consistent with the decrease in the total number of
333 synapses per myotome leading to insufficient activation of the myotome.

334 **DISCUSSION**

335 Mutations, including loss-of-function mutations, in Fmn2 have been associated with
336 intellectual disability, sensory dysfunction, age-associated cognitive decline (Perrone
337 et al., 2012; Law et al., 2014; Agís-Balboa et al., 2017; Marco et al., 2018; Gorukmez
338 et al., 2020). Interestingly, some affected individuals also develop hypotonia (Law et
339 al). Further, mutations in Fmn2 have also been associated with sporadic amyotrophic
340 lateral sclerosis in multiple studies (Schymick et al., 2007; Pamphlett et al., 2011;
341 Morello et al., 2018). These associations suggest a possible involvement of Fmn2 in
342 motor neuron development and function.

343 In this study, we generated *fmn2b* mutants using the CRISPR-Cas9 system (Figure 1)
344 and found locomotor deficits in the homozygous mutants. *The fmn2b* mutants
345 displayed deficits right from the earliest motor behaviours (STC at 22 hpf; Figure 2) to
346 later stages where the development of the embryonic neural circuits is complete
347 (TEER at 60 hpf; Figure 2). *fmn2b* mRNA expression was also detected in motor
348 neurons and the spinal cord (Figure 3). Systematic evaluation of the primary motor
349 neurons revealed defects in the outgrowth of the CaP motor neurons. Live imaging
350 indicated that the growth cone translocation velocity was reduced in *fmn2b*$^{\Delta 4/\Delta 7}$
351 embryos (Figure 3).

352 Recent *in vitro* studies in chick spinal neurons implicates Fmn2 in growth cone
353 translocation. These studies implicate Fmn2 in mediating a molecular clutch that
354 stabilizes the contact sites between the growth cone and the extracellular matrix and
355 regulates the generation of traction forces required for outgrowth (Sahasrabudhe et
356 al., 2016; Ghate et al., 2020). Additionally, Fmn2 facilitates the stabilization of
357 protrusive processes, like growth cone filopodia, by coupling exploratory microtubules

358 with the F-actin cytoskeleton (Kundu et al., 2021). Consistent with this, the depletion
359 of Fmn2 reveals altered microtubule dynamics in the growth cones of zebrafish Rohon-
360 Beard neurons *in vivo*. Similar mechanisms involving actin and microtubule
361 remodelling could be involved in the translocation of CaP growth cones in zebrafish.

362 Even more striking than the delayed outgrowth rates of CaP motor neurons, the
363 development of collateral branches which provide synaptic coverage of the entire
364 muscle field was severely affected (Figure 4). The staggered development of motor
365 neurons in two phases allowed us to selectively look at the innervation of muscles by
366 primary motor neurons at 24 hpf and collectively look at primary and secondary motor
367 neuron innervation at 60 hpf. In addition, the 60 hpf embryos have elaborate branching
368 and fully functional NMJ synapses allowing characterization of *fmn2b* in outgrowth,
369 branching and synapse formation in motor neurons.

370 In 24 hpf *fmn2b* mutant embryos, branch density along the fascicle extended by the
371 primary motor neurons and the fascicle length itself was reduced, suggesting a
372 decrease in the innervation of the target fast muscle fibers (Figure 4). Similarly, the 60
373 hpf *fmn2b*$^{\Delta 4/\Delta 7}$ embryos have reduced branch density and fascicle outgrowth
374 compared to wild-type embryos and are likely to result in reduced speed and distance
375 covered by *fmn2b* mutants (Figure 4). Deficits in motor neuron outgrowth and collateral
376 branching at both 24 hpf and 60 hpf was rescued by overexpressing mouse full length
377 Fmn2 in the *fmn2b* homozygous mutants (Figure 4).

378 Axon collateral branching is a finely regulated multi-step process initiated by the rapid
379 assembly of F-actin resulting in a filopodia-like protrusion from the axonal shaft
380 (Ketschek and Gallo, 2010; Gallo, 2011, 2016; Coles and Bradke, 2015; Ketschek et
381 al., 2015; Armijo-Weingart and Gallo, 2017; Menon and Gupton, 2018). Further
382 cytoskeleton remodelling involving both the actin and microtubule cytoskeletons

383 stabilize the protrusion and extend it to a collateral branch (Gallo, 2011, 2016; Armijo-
384 Weingart and Gallo, 2017). The formation of the lateral protrusion from the axonal
385 shaft is a major rate-limiting step in collateral branching and is initiated by the
386 development of a juxtamembrane F-actin patch. *In vitro* studies implicate several actin
387 binding proteins in regulating axonal F-actin patches. These include the actin
388 nucleating Arp2/3 complex, Drebrin, WVE-1/WAVE regulatory complex (WRC) and
389 cortactin (Spillane et al., 2011; Hu et al., 2012; Chia et al., 2014; Spillane and Gallo,
390 2014; Ketschek et al., 2016; Balasanyan et al., 2017). Recently, Fmn2 has been
391 implicated in collateral branch formation in chick spinal neurons *in vitro*. Fmn2 appears
392 to regulate the lifetime of axonal F-actin patches and consequently the probability of
393 branch initiation (Kundu et al., 2020).

394 The F-actin nucleation and elongation activity of Fmn2 has been characterized *in vitro*
395 (Montaville et al., 2014, 2016). Abrogation of F-actin nucleation activity of Fmn2 can
396 be achieved by mutating a conserved Isoleucine residue in the FH2 domain to Alanine
397 (Quinlan et al., 2007; Roth-Johnson et al., 2014; Kundu et al., 2020). We employed
398 the full-length mouse Fmn2 bearing the isoleucine to alanine mutation (mFmn2-
399 I1226A) in rescue experiments to test if the F-actin nucleating/elongating activity is
400 necessary for motor neuron development.

401 Expression of mFmn2-I1226A in the *fmn2b* mutants could not rescue the outgrowth
402 and branching defects of the motor neurons in 24 hpf and 60 hpf embryos (Figure 4).
403 The failure of mFmn2-I1226A in rescuing the defects underscores the significance of
404 the actin nucleating activity of Fmn2b in motor neuron outgrowth and branching
405 consistent with reports from primary neuronal cultures of chick spinal cord reported
406 previously (Kundu et al., 2020). Therefore, the motor neuron development in zebrafish
407 is dependent on the F-actin nucleation activity of Fmn2b.

408 Loss of fmn2b had pleiotropic effects on the development of the RoP motor neuron.
409 The RoP soma and RoP outgrowth were severely affected in *fmn2b* mutants. At 24
410 hpf, multiple hemisegments in *fmn2b* mutants did not have RoP soma at its
411 characteristic position in the spinal cord (Figure 5). The role of Fmn2 in the regulation
412 of differentiation or specification of progenitors is not formally tested despite several
413 studies indirectly indicating pathways involving Fmn2 in cell differentiation. In a recent
414 report, Fmn2 has been shown to cause neural progenitor differentiation defects Fmn2
415 and Flna double knockout mice in a synergistic manner (Lian et al., 2016). The
416 absence of RoP soma in zebrafish *fmn2b* mutants may indicate a possible role of
417 *fmn2b* in neural progenitor specification and/or differentiation. The RoP soma was
418 seen in the expected location in *fmn2b*$^{\Delta 4/\Delta 7}$ embryos injected with mFmn2 mRNA but
419 the defect could not be rescued by the injection of mFmn2-I1226A mRNA.
420 Interestingly, the F-actin nucleating activity of Fmn2 is required for the differentiation
421 of motor neuron progenitors or their specification. These results open up new
422 possibilities to uncover the mechanistic role of Fmn2 in neural development.

423 In wild-type zebrafish embryos, the lateral projections from RoP motor neurons and
424 follower secondary motor neurons begin outgrowth later than CaP and MiP neurons
425 (Kuwada, 1993; Liu et al., 2016). In 60 hpf *fmn2b* mutants, the side branches of RoP
426 motor neurons innervating the horizontal myoseptum were either not detected (46%
427 embryos) or appeared to be stalled at the choice point (44% embryos), i.e., the
428 horizontal myoseptum (Figure 5). RoP-like secondary motor neurons, which follow the
429 same trajectory as RoP primary motor neurons have previously been shown to have
430 pathfinding and stalling defects at the horizontal myoseptum in Fidgetin like-1 and
431 Kif1b mutants (Fassier et al., 2018; Atkins et al., 2019). Similarly, the stalled RoP
432 axons appear defasciculated in 60 hpf *fmn2b* mutants

433 One of the factors contributing to RoP outgrowth defects leading to the absence of
434 RoP innervation in *fmn2b* mutants could be the lack of RoP soma as seen in 24 hpf
435 mutant embryos. Further, the RoP stalling defect implicates Fmn2b in axonal
436 pathfinding in response to guidance cues at the choice point. RoP outgrowth and
437 stalling together caused a noticeable reduction in the innervation of the mid-dorsal and
438 mid-ventral region of the axial myotome. The RoP may be more severely affected than
439 the CaP neurons due to their late axonogenesis concomitant with the pleiotropic
440 function and late expression of *fmn2b* in the spinal cord at 48 hpf.

441 Intriguingly, the overexpression of mouse Fmn2 in *fmn2b*$^{+/+}$ (wild-type) embryos
442 causes opposite effects as compared to *fmn2b* knockout manifested as
443 hyperbranching. This implies a significant role for *fmn2b* in regulating the collateral
444 branching of motor neurons. Further, overexpression of the nucleation dead version
445 of mFmn2 does not result in increased branch density and underscores the
446 involvement of actin nucleation activity of Fmn2 (Figure 6).

447 Analysis of NMJ synapses using znp-1 and α-bungarotoxin double staining in *fmn2b*
448 mutants showed no changes in the number of synapses along the total length of the
449 motor neuron branches but showed a reduction in the total number of synapses when
450 normalized to the area of the target myotome. We suggest that the Fmn2b has a
451 primary role in regulating motor neuron branching and not in the formation of NMJ
452 synapses. The behavioural defects in *fmn2b* mutants are likely due to the muscles not
453 receiving sufficient input due to inadequate branching (Figure 7).

454 In a recent study, prolonged exposure of zebrafish larvae to strong and variable water
455 currents caused upregulation of Fmn2b (Langebeck-Jensen et al., 2019). The rapid
456 upregulation of Fmn2b in response to environmental stressors involving swimming and
457 force generation in larvae with pre-established motor neural circuits invoke the

458 possible involvement of *fmn2b* in neuronal plasticity and requires systematic
459 investigation.

460 Taken together, the zebrafish model of Fmn2 loss-of-function offers unexpected
461 insight into motor neuron development and innervation of axial muscles. In addition to
462 identifying the requirement of actin polymerization by Fmn2 in motor neuron
463 morphogenesis and motor outputs, it highlights the central role of cytoskeleton
464 remodelling in motor neuron homeostasis and the development of neuropathies.

465 **CONCLUSIONS**

466 Motor behaviours like spontaneous tail coiling and touch evoked escape response
467 were adversely affected in the *fmn2b* mutants. Visualizing developing motor neurons
468 using the *Tg(mnx1:GFP)* in *fmn2b* mutants revealed outgrowth and branching defects
469 but no changes to myotome integrity. Further, we find that the F-actin nucleating
470 activity of Fmn2 is required for motor neuron outgrowth and collateral branching. The
471 reduced coverage of the axial myotomes by the motor neurons results in compromised
472 synaptic inputs and contributes to the motor deficits observed in the *fmn2b* mutants.

473 # METHODS

474 **Zebrafish maintenance and procedures**

475 All protocols used in this study were approved by the Institutional Animal Ethics
476 Committee and the Institutional Biosafety Committee of IISER Pune or a National
477 Human Genome Research Institute (NHGRI/NIH) Animal Care and Use Committee
478 approved animal study protocol. The TAB5 wildtype strain of zebrafish was used for
479 all the experiments including generation of CRISPR mutants. The TAB5 strain was
480 used for all the wildtype outcrosses. Breeding pairs of adult zebrafish were maintained
481 in recirculating aquaria (Techniplast) under a 14h-10h light-dark cycle. The
482 temperature was maintained at 28.5˚C and the pH was buffered between 7.2 to 7.8.
483 The breeding adults were crossed to obtain embryos which were collected and grown
484 in E3 buffer and used at different stages of development as indicated (Kimmel et al.,
485 1995). For immunostaining and live imaging experiments, the buffer was
486 supplemented with 0.003% Phenylthiourea (PTU; Sigma) to remove pigmentation
487 from the skin. The transgenic line *Tg(mnx1:GFP)* was used to visualize motor neurons
488 wherein the *mnx1* promoter specific to motor neurons drives GFP expression
489 (Flanagan-Steet et al., 2005).

490 **Whole mount in situ hybridization**

491 The RNA probes and procedure used for whole mount *in situ* hybridization
492 experiments have been described previously (Nagar et al., 2021).

493 **Isolation of motor neurons from transgenic embryos, FACS, RT-PCR**

494 Single cell suspension was made from around 200 *Tg(mnx1:GFP)* embryos as
495 previously described (Bresciani et al., 2018). Briefly, the embryos were dissociated by
496 trypsinization and filtering through a 70 µm sieve to obtain single cell suspension in

497 1X DMEM containing 10% FBS. The cells were sorted using a BD Biosciences
498 fluorescence-activated cell sorting (FACS) equipment selecting cells expressing GFP,
499 i.e., the motor neurons. RNA was extracted using Qiagen RNeasy Kit and cDNA was
500 prepared using the SuperScript IV RT Kit (ThermoFisher). The cDNA was used for
501 amplifying *fmn2b* transcripts in the mnx1 positive motor neurons. Primers and PCR
502 protocol used to test the presence of *fmn2b* transcripts in motor neurons tagged by
503 *Tg(mnx1:GFP)* were the same as the ones used for amplification of ISH probes from
504 cDNA.

505 **RNA injections**

506 Capped mRNA was synthesized using the HiScribe™ T7 ARCA mRNA Kit (with
507 tailing) from linearized DNA template containing T7 promoter sequence upstream of
508 the mFmn2-mCherry and mFmn2-I1226A-mCherry constructs. The transcribed mRNA
509 was purified using RNeasy MinElute Cleanup Kit (Qiagen). 150 pg of mFmn2-mCherry
510 and mFmn2-I1226A-mCherry mRNA was injected in the zebrafish embryos of desired
511 genotype at 1-cell stage.

512 **sgRNA and Cas9 injections for CRISPR mutants**

513 sgRNA targeting exon 1 of *fmn2b* was designed as previously described (Varshney et
514 al., 2016). T7 HiScribe kit (NEB) was used to transcribe the sgRNA DNA template with
515 the appended T7 promoter. The sgRNA was purified using ZymoResearch clean up
516 columns. T3 mMessage mMachine RNA synthesis kit (Ambion) was used to
517 synthesize capped Cas9 mRNA from the pT3TS-nCas9n plasmid (kind gift from Dr
518 Wenbiao Chen; Addgene plasmid # 46757). The synthesized Cas9 mRNA was
519 purified using the RNeasy MinElute Cleanup Kit (Qiagen). 30 pg sgRNA and 300 pg

520 Cas9 mRNA was injected in zebrafish embryos at 1 cell stage. The sequence of
521 sgRNA is given below.

522 Fmn2b_sgRNA : GGGCGAGAGGCCTCGGCTGG

523 (ENSDARG00000061778.6; 12:47451436-47451459, plus strand)

524 **Genotyping CRISPR mutants**

525 For identifying founder lines for *fmn2b* mutants, fluorescent PCR was performed and
526 analyzed by capillary gel electrophoresis using the ABI GeneAnalyzer 3730XL, as
527 previously described (Carrington et al., 2015; Varshney et al., 2015, 2016).
528 Identification of homozygous mutant lines was also done using Sanger sequencing.
529 Two zebrafish mutant lines with alleles causing a premature stop codon due to a
530 frameshift mutation were established. The homozygous mutants were crossed to each
531 other to obtain a heteroallelic mutant line for *fmn2b* to reduce the effect of any
532 background mutations in the two mutant lines due to unintended off-target effects.
533 Primer sequences for sanger sequencing of genomic DNA amplicons from crispants
534 are as follows:

Fmn2b_PCR_F	AAGCGTAAGAACCAGAATAAGC
Fmn2b_PCR_R	TCATCCGAATGGCTTGC

535

536 **Whole mount immunostaining**

537 PTU treated embryos were collected at desired stages and fixed in 4% formaldehyde
538 overnight at 4˚C. For staining actin structures, fixed embryos were washed with 0.5%
539 PBS-Triton, permeabilized with 2% PBS-Triton for 2 hours at room temperature and

540 then incubated in Phalloidin Alexa Fluor 568 diluted 1:50 in 2% PBS Triton overnight
541 at 4 °C in dark.

542 **Neuromuscular junction labelling and quantification**

543 For neuromuscular junction staining of embryos, znp-1 antibody (DSHB; 1:100) and
544 Tetramethyl Rhodamine labelled α-bungarotoxin (Invitrogen; 1:200) were used as pre-
545 synaptic and post-synaptic markers respectively. Whole mount immunostaining
546 procedures described in previous section were followed as described. The synapses
547 were counted using the SynapCountJ plugin after making the traces of arbours in
548 NeuronJ plugin in Fiji.

549 **Fluorescence microscopy, live imaging and mounting procedure**

550 All the microscopic imaging was performed on the inverted LSM 780 confocal
551 microscope (Zeiss) with a 25x oil immersion objective (NA 1.4). For imaging of the
552 fixed samples, the embryos were cleared in 50% glycerol and mounted dorsal side
553 down on a glass bottom petri dish using low gelling agarose (Sigma). For live imaging,
554 the live embryos were mounted laterally in 0.5% low melt point agarose (Sigma)
555 containing 0.003% MS-222 (Sigma) in a coverslip bottom 35 mm petri plate.

556 The growth cone of motor neurons was visualized using the *Tg(mnx1:GFP)* in wildtype
557 or mutant background. The embryos were imaged starting at 22 hpf for 4-6 hours every
558 3 minutes. The growth cone translocation was analyzed using the Manual tracking
559 plugin in Fiji to track the movement of the leading edge across time. The coordinates
560 obtained were analyzed using the ibidi Chemotaxis tool to calculate the average
561 growth cone translocation speed.

562 **Behaviour experiment set up and behaviour analysis**

563 *Spontaneous tail coiling (STC) assay*

564 Embryos 22 hpf within their chorions were transferred to a 35 mm petri plate containing
565 E3 buffer at of 28.5˚C. A video camera (AVT Pike, F-032B) was used to record the
566 spontaneous tail coiling behaviour of the embryos for a time period of 3 minutes at 15
567 fps. The videos were processed and analysed using a MATLAB script ZebraSTM
568 published previously (González-Fraga et al., 2019).

569 *Touch evoked escape response (TEER) assay*

570 60 hpf zebrafish embryos were housed in a 35 mm petri plate containing pre-warmed
571 E3 buffer at 28.5 ˚C. A tuberculin needle was repurposed by attaching a soft nylon
572 fiber in front of the syringe holding the needle, to deliver tactile stimuli to zebrafish
573 embryos. A soft touch was delivered to the head of the zebrafish once and their
574 behaviour was recorded using a high-speed video camera (AVT Pike F-032B) at 208
575 fps. The videos obtained were analyzed using the Manual tracking plugin in Fiji to mark
576 the trajectories of the zebrafish embryos upon receiving the tactile stimulus. The tracks
577 were further analyzed using the ibidi Chemotaxis tool to calculate the distance
578 travelled and average speed. The maximum instantaneous speed was calculated
579 manually from the coordinates obtained from the manual tracking output.

580 **Figures and Statistical analysis**

581 The analysis was performed for all the experiments in a genotype blinded manner.
582 Image analysis was performed using Fiji and the Figure panels were assembled using
583 Inkscape. The Violin plots were plotted in GraphPad Prism 8 and indicated statistical
584 tests were performed using GraphPad Prism 8. The data is represented as mean ±
585 SEM in the text. The statistical test used and the p values are indicated in the Figure
586 legends.

587

AVAILABILITY OF DATA AND MATERIALS

The data generated and analyzed in this study are included in this article and the additional information files. More information can be made available upon reasonable request to the corresponding author.

592 **FIGURES**

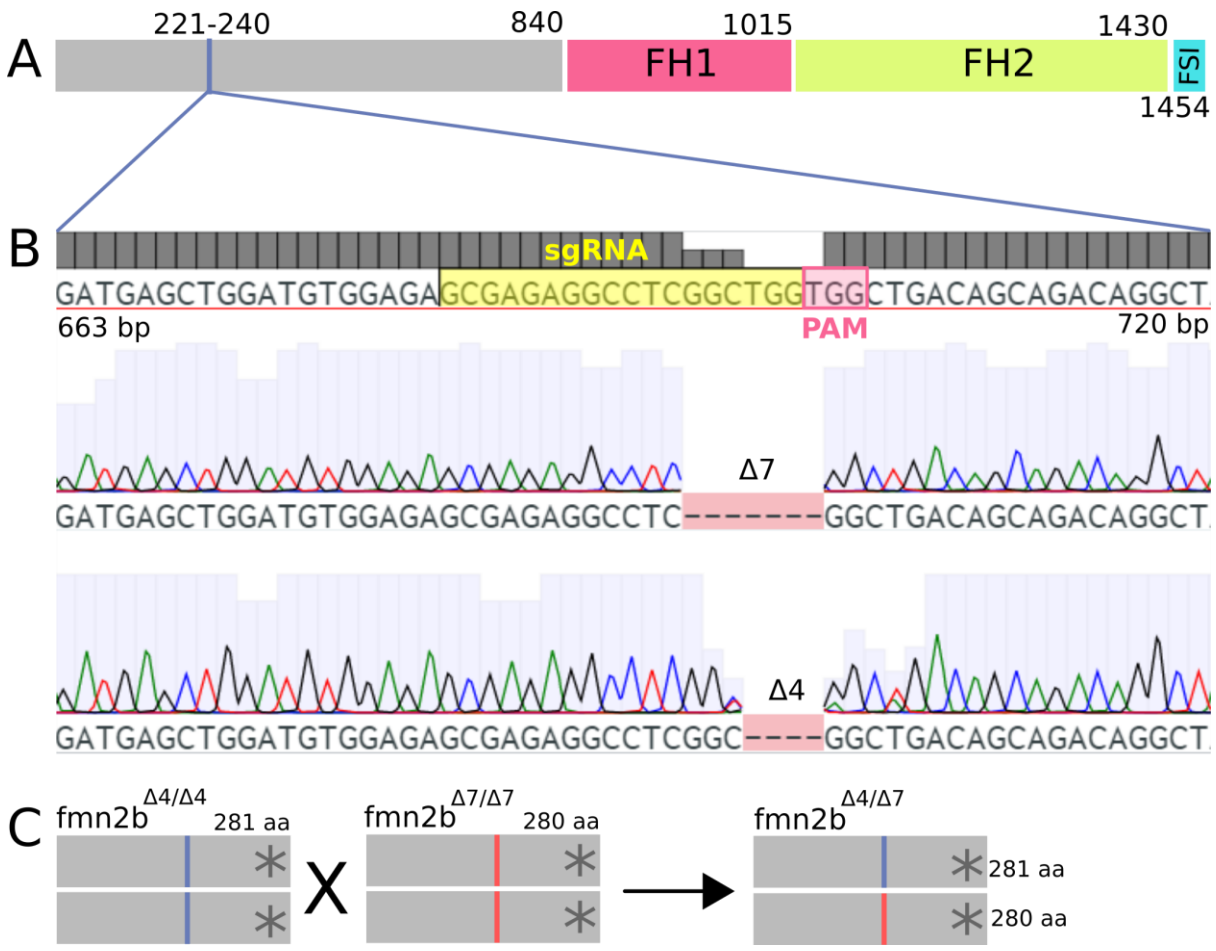

593

594 **Figure 1. Generation of *fmn2b* CRISPR mutants. A)** Schematic of the *fmn2b* protein
595 indicating the functional protein domains and the site of *fmn2b* sgRNA-1. The FH1
596 domain spans the 841-1015 amino acids, FH2 domain spans the 1016-1430 amino
597 acids and the FSI domain spans the 1431-1454 amino acids. **B)** Genomic locus from
598 *fmn2b* exon 1 starting from 663 bp to 720 bp (corresponding to 221-240 amino acids).
599 The sgRNA sequence is highlighted in yellow followed by the PAM sequence in pink.
600 Representative chromatograms of amplicons sequenced from homozygous CRISPR
601 mutants for *fmn2b* show two alleles with a 7 bp and a 4 bp deletion, respectively. The
602 two alleles are denoted as *fmn2b*$^{\Delta 7}$ and *fmn2b*$^{\Delta 4}$. **C)** Schematic outlining the generation
603 of *fmn2b* homozygous mutants. Fish homozygous for two alleles are denoted as
604 *fmn2b*$^{\Delta 7/\Delta 7}$ and *fmn2b*$^{\Delta 4/\Delta 4}$, the heteroallelic combination is denoted as *fmn2b*$^{\Delta 4/\Delta 7}$.

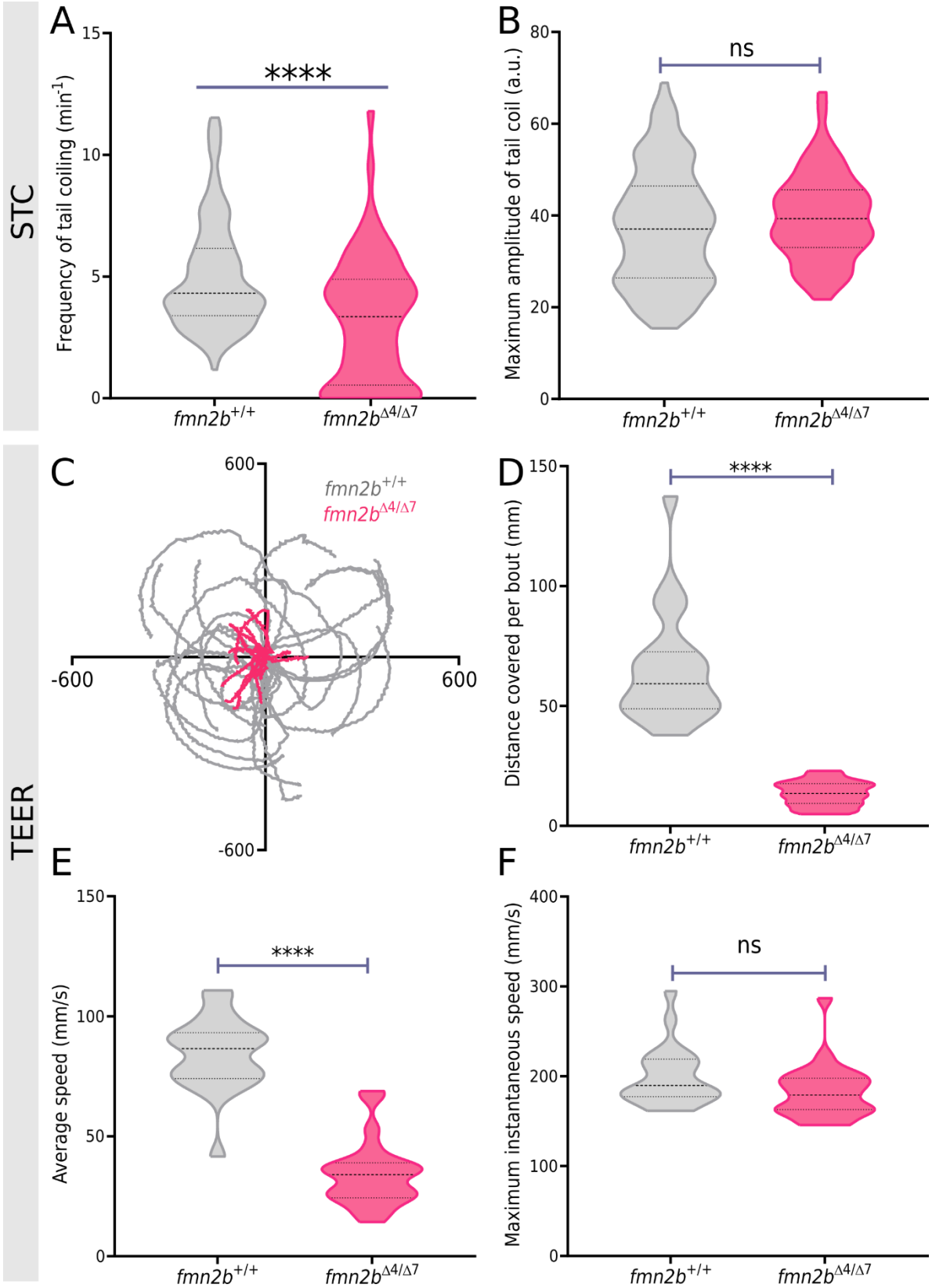

605

606 **Figure 2. *fmn2b* mutants exhibit motor defects. A)** Spontaneous tail coiling (STC)

607 frequency and **B)** maximum amplitude of tail coiling in 22 hpf *fmn2b*$^{+/+}$ (n=121) and

608 *fmn2b*$^{\Delta 4/\Delta 7}$ (n=68) embryos. **C)** Trajectories of 2 dpf *fmn2b*$^{+/+}$ (grey traces; n=22) and
609 *fmn2b*$^{\Delta 4/\Delta 7}$ (pink traces; n=24) embryos in Touch Evoked escape response (TEER),
610 re-centered to a common origin for representation. The x and y axes in the plot
611 correspond to the pixel values corresponding to coordinates of the fish from
612 consecutively acquired frames. Quantification of **D)** distance covered per swim bout,
613 **E)** average speed during the swim bout, and **F)** maximum instantaneous swimming
614 speed of 2 dpf *fmn2b*$^{+/+}$ (n=22) and *fmn2b*$^{\Delta 4/\Delta 7}$ (n=24) embryos in response to a tactile
615 stimulus. (**** p-value <0.0001; ns- not significant; Mann-Whitney U test)

616

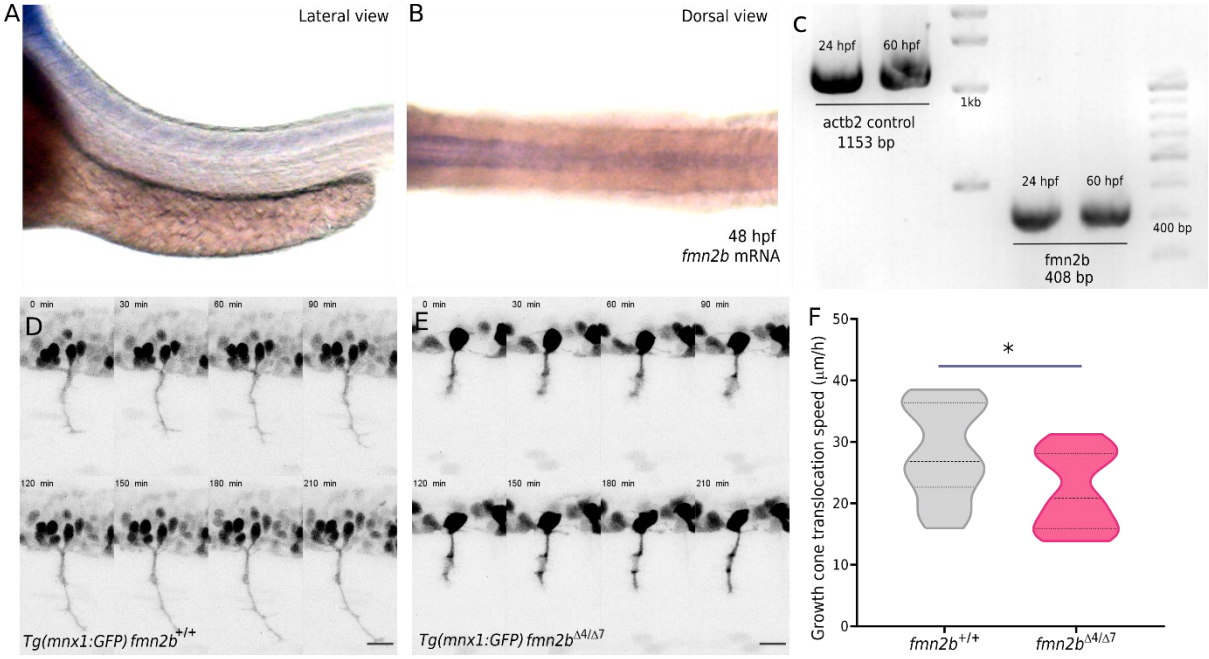

Figure 3. *fmn2b* is expressed in the spinal cord and motor neurons of zebrafish embryos. *fmn2b* is required for motor neuron growth cone translocation

A) Lateral and **B)** dorsal views of a representative 60 hpf embryo showing *fmn2b* mRNA expression in the spinal cord. **C)** Gel showing bands for amplified β2-actin (actb2) control and *fmn2b* from cDNA obtained from FACS sorted motor neurons (mnx1:GFP positive cells) isolated from 24 hpf and 60 hpf wild-type *Tg(mnx1:GFP)* embryos. **D)** Representative montages of live imaging of growth cone translocation in *fmn2b*$^{+/+}$ and **E)** *fmn2b*$^{\Delta 4/\Delta 7}$ embryos in the background of *Tg(mnx1:GFP)* during the time period of 22 hpf to 26 hpf. **F)** Quantification of motor neuron growth cone translocation speed in *fmn2b*$^{+/+}$ (n=15 growth cones; N=3 embryos) and *fmn2b*$^{\Delta 4/\Delta 7}$ (n=16 growth cones; N=4 embryos). (* p-value = 0.0298; Mann-Whitney U test). Scale bar is equivalent to 20 µm.

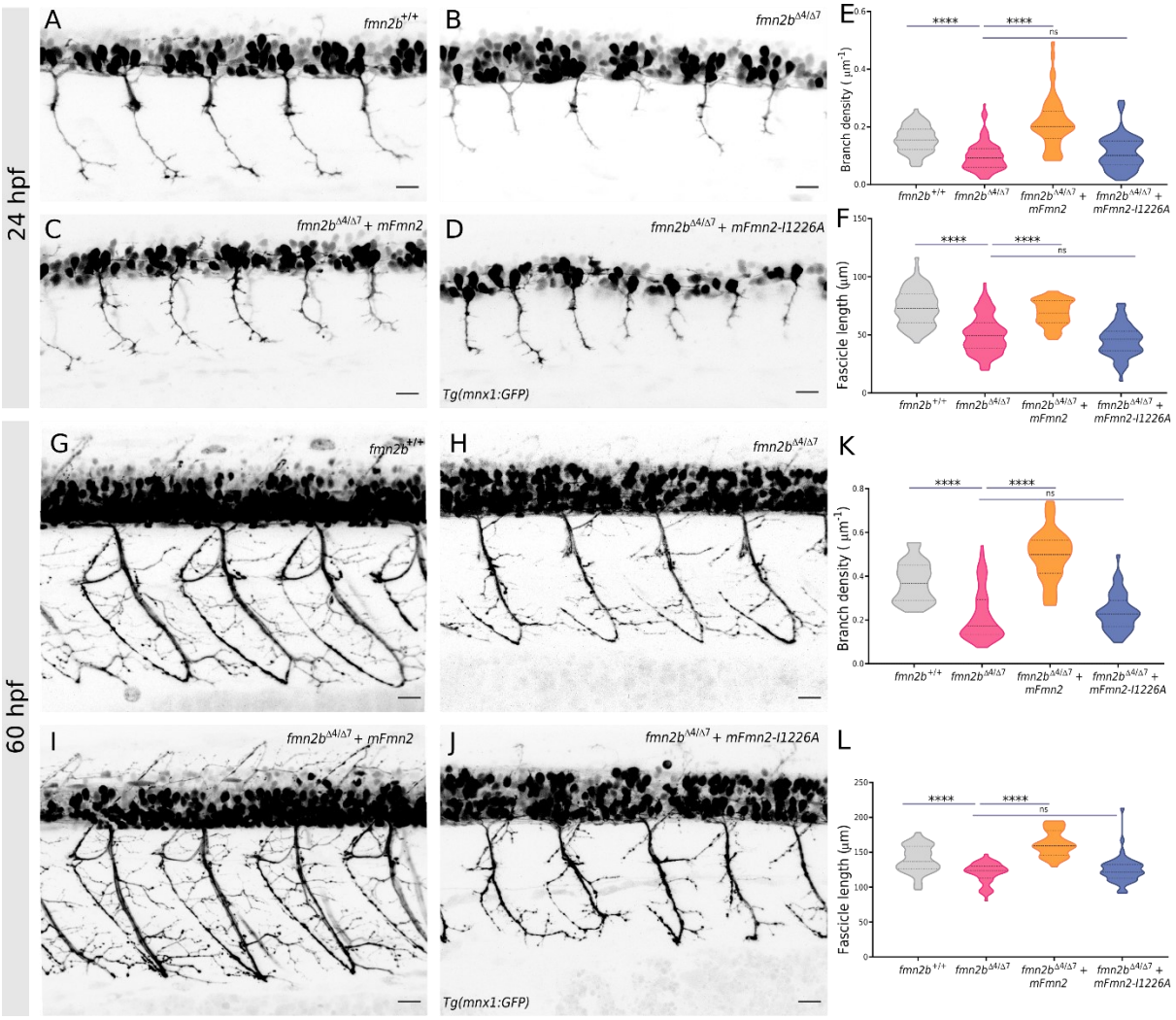

Figure 4. Motor neuron outgrowth and branching defects in *fmn2b* mutants

Representative micrographs of motor neurons labelled by *Tg(mnx1:GFP)* in 24 hpf **A)** *fmn2b*$^{+/+}$ and **B)** *fmn2b*$^{\Delta4/\Delta7}$ and 60 hpf **G)** *fmn2b*$^{+/+}$ and **H)** *fmn2b*$^{\Delta4/\Delta7}$ embryos. Motor neurons visualized by *Tg(mnx1:GFP)* in *fmn2b*$^{\Delta4/\Delta7}$ mutant embryos injected at 1-cell stage with full-length mouse Fmn2 (mFmn2) mRNA at **C)** 24 hpf and **I)** 60 hpf and nucleation dead mouse Fmn2 (mFmn2-I1226A) mRNA at **D)** 24 hpf and **J)** 60 hpf. **E)** Quantification of branch density (number of branches per fascicle normalized to the fascicle length) per myotome hemisegment in 24 hpf *fmn2b*$^{+/+}$ (0.1571 ± 0.005 µm^{-1}; n=70 hemisegments) and *fmn2b*$^{\Delta4/\Delta7}$ embryos (0.0981 ± 0.005 µm^{-1}; n=118 hemisegments). The defects were rescued in *fmn2b*$^{\Delta4/\Delta7}$ embryos injected with

642 mFmn2 mRNA (0.2139 ± 0.012 μm^{-1}; n=51 hemisegments) but not in the embryos
643 injected with mFmn2-I1226A mRNA (0.111 ± 0.007 μm^{-1}; n=63 hemisegments). **F)**
644 Quantification of fascicle length extended by motor neurons per myotome
645 hemisegment in 24 hpf *fmn2b*$^{+/+}$ (68.97 ± 1.55 µm; n=70 hemisegments) and
646 *fmn2b*$^{\Delta 4/\Delta 7}$ embryos (44.98 ± 1.756 µm; n=118 hemisegments). The defects were
647 rescued in *fmn2b*$^{\Delta 4/\Delta 7}$ embryos injected with mFmn2 mRNA (73.7 ± 1.86 µm; n=51
648 hemisegments) but not in the embryos injected with mFmn2-I1226A mRNA (73.7 ±
649 1.86 µm; n=63 hemisegments). **K)** Quantification of branch density (number of
650 branches per fascicle normalized to the fascicle length) per myotome hemisegment in
651 60 hpf *fmn2b*$^{+/+}$ (0.3746 ± 0.014 μm^{-1}; n=37 hemisegments) and *fmn2b*$^{\Delta 4/\Delta 7}$ embryos
652 (0.2211 ± 0.015 μm^{-1}; n=57 hemisegments). The defects were rescued in *fmn2b*$^{\Delta 4/\Delta 7}$
653 embryos injected with mFmn2 mRNA (0.4955 ± 0.021 μm^{-1}; n=30 hemisegments) but
654 not in the embryos injected with mFmn2-I1226A mRNA (0.2369 ± 0.012 μm^{-1}; n=48
655 hemisegments). **L)** Quantification of fascicle length extended by motor neurons per
656 myotome hemisegment in 60 hpf *fmn2b*$^{+/+}$ (139.6 ± 3.21 µm; n=37 hemisegments) and
657 *fmn2b*$^{\Delta 4/\Delta 7}$ embryos (120.4 ± 1.94 µm; n=57 hemisegments). The defects were
658 rescued in *fmn2b*$^{\Delta 4/\Delta 7}$ embryos injected with mFmn2 mRNA (162.7 ± 3.38 µm; n=30
659 hemisegments) but not in the embryos injected with mFmn2-I1226A mRNA (124.7 ±
660 2.81 µm; n=48 hemisegments). (**** p-value <0.0001; ns - not significant; Kruskal
661 Wallis test followed by Dunn's post-hoc analysis). Scale bar is equivalent to 20 µm.

662

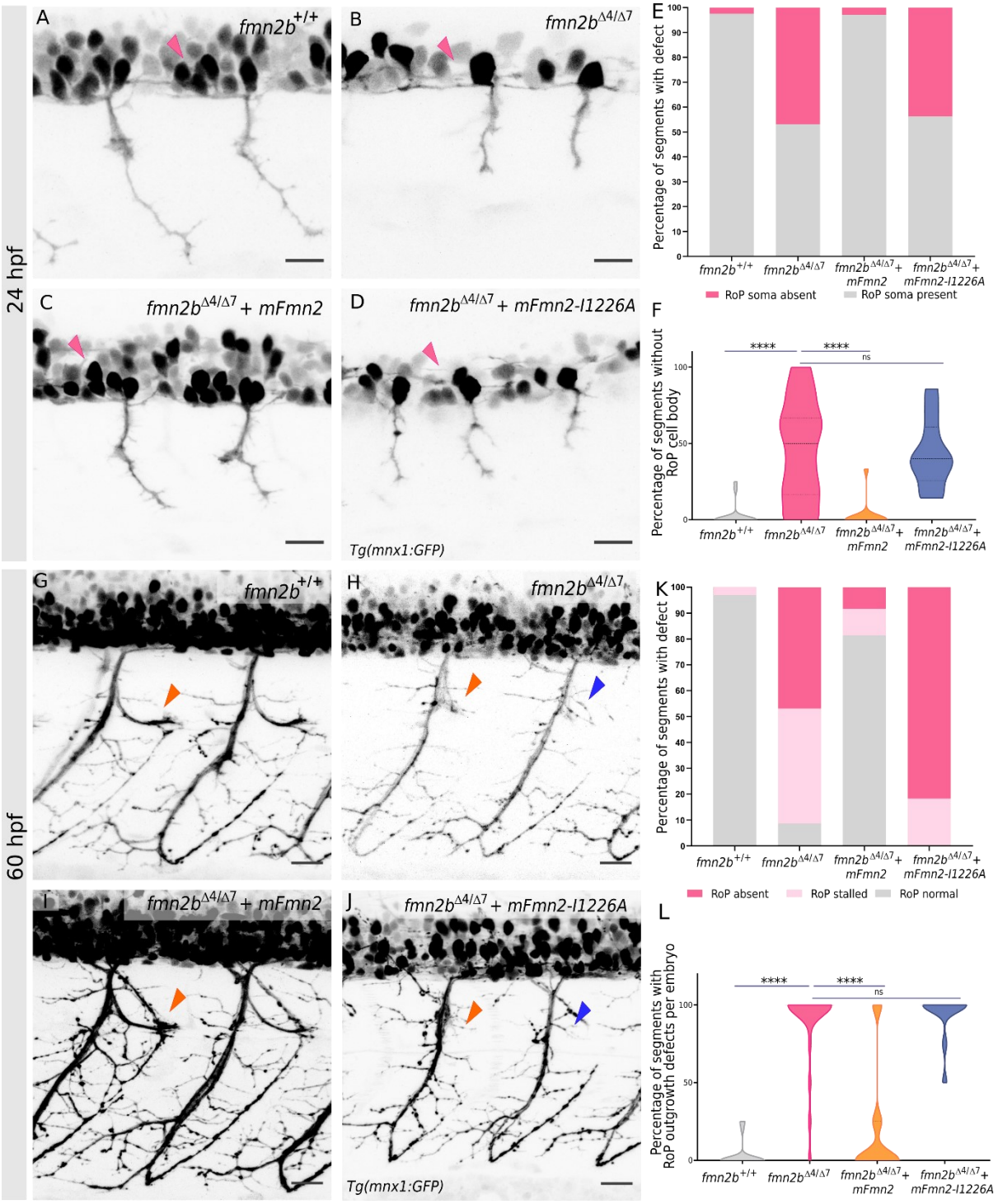

663

664 **Figure 5. RoP soma and lateral innervation of the myotome by RoP are affected**

665 **in *fmn2b* mutants**

666 Representative micrographs of motor neurons labelled by *Tg(mnx1:GFP)* in 24 hpf **A)**

667 *fmn2b*$^{+/+}$ and **B)** *fmn2b*$^{\Delta4/\Delta7}$ embryos. Representative micrographs of motor neurons

668 labelled by *Tg(mnx1:GFP)* in 24 hpf old *fmn2b*$^{\Delta4/\Delta7}$ mutant embryos injected at 1-cell

669 stage with **C)** full-length mouse Fmn2 (mFmn2) mRNA and **D)** nucleation dead
670 version, mFmn2-I1226A mRNA. The pink arrowheads indicate the RoP soma or its
671 expected position. **E)** Bar graph summarizing the percentage of embryos with defects
672 in RoP soma in 24 hpf *fmn2b*$^{+/+}$ (n=18) and *fmn2b*$^{\Delta 4/\Delta 7}$ embryos (n=23). The defects
673 were rescued in *fmn2b*$^{\Delta 4/\Delta 7}$ embryos injected with mFmn2 mRNA (n=12) but not in the
674 embryos injected with mFmn2-I1226A mRNA (n=10*).* χ2 test of independence shows
675 significant difference between the four groups, $\chi 2$ (df = 3) =101.8 , $p < 0.0001$. **F)** Violin
676 plots depicting the variation in data summarized in the bar graphs for 24 hpf embryos.
677 (**** p-value <0.0001; ns - not significant; Kruskal Wallis test followed by Dunn's post-
678 hoc analysis). Scale bar is equivalent to 20 μm.

679 Representative micrographs of motor neurons labelled by *Tg(mnx1:GFP)* in 60 hpf **G)**
680 *fmn2b*$^{+/+}$ and **H)** *fmn2b*$^{\Delta 4/\Delta 7}$ embryos. Representative micrographs of motor neurons
681 labelled by *Tg(mnx1:GFP)* in 60 hpf old *fmn2b*$^{\Delta 4/\Delta 7}$ mutant embryos injected at 1-cell
682 stage with **I)** full-length mouse Fmn2 (mFmn2) mRNA and **J)** nucleation dead version,
683 mFmn2-I1226A mRNA. The orange arrowheads point towards the stalled RoP and the
684 blue arrowheads indicate no RoP outgrowth. **K)** Bar graphs summarizing the
685 percentage of embryos with defects in RoP axon outgrowth in 60 hpf *fmn2b*$^{+/+}$ (n=22)
686 and *fmn2b*$^{\Delta 4/\Delta 7}$ embryos (n=26). The defects were rescued in *fmn2b*$^{\Delta 4/\Delta 7}$ embryos
687 injected with mFmn2 mRNA (n=14) but not in the embryos injected with mFmn2-
688 I1226A mRNA (n=13). χ2 test of independence shows significant difference between
689 the four groups, $\chi 2$ (df = 6) = 332.7, $p < 0.0001$. **L)** Violin plots depicting the variation
690 in data summarized in the bar graphs for 60 hpf embryos. (**** p-value <0.0001; ns -
691 not significant; Kruskal Wallis test followed by Dunn's post-hoc analysis) Scale bar is
692 equivalent to 20 μm.

693

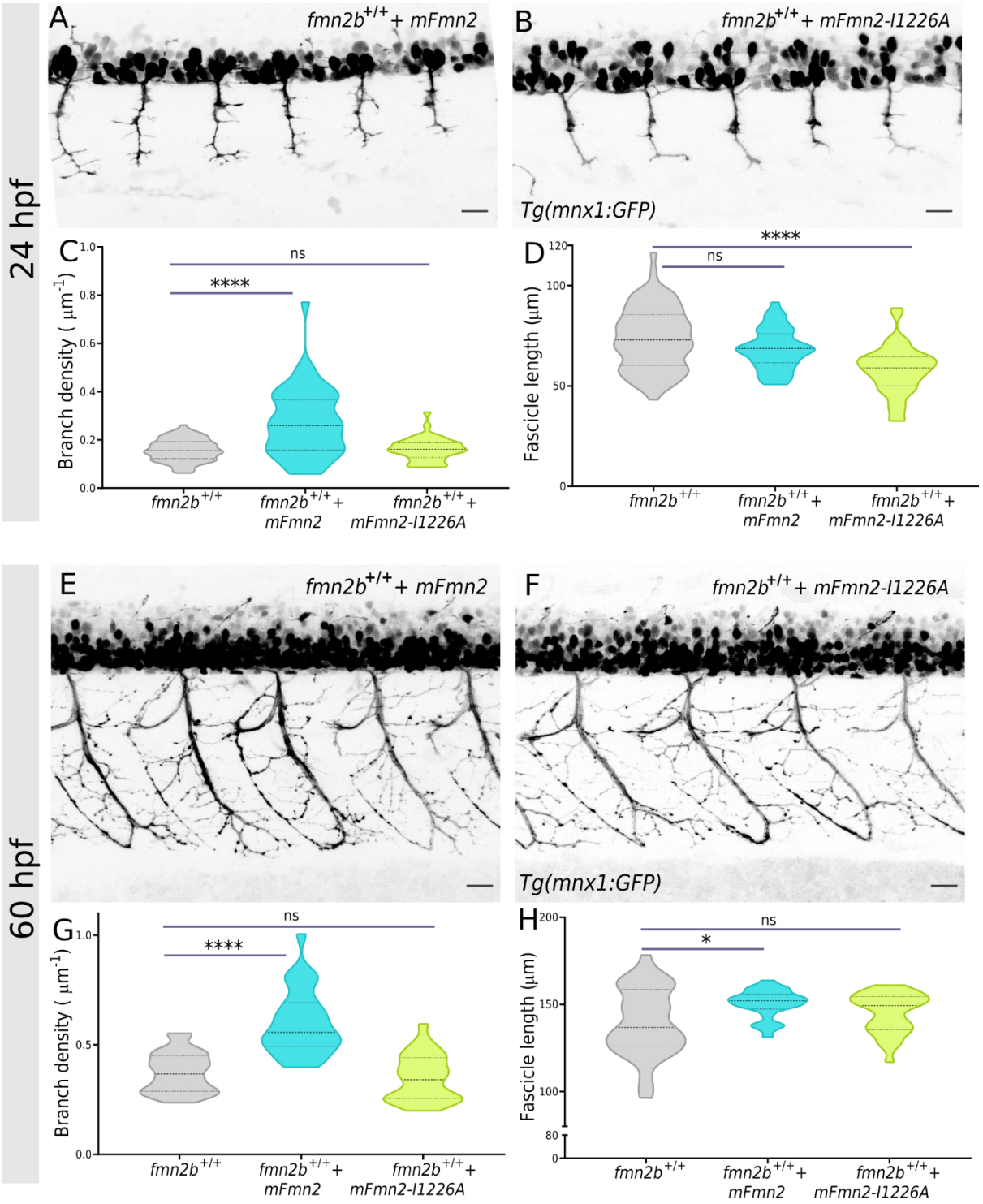

Figure 6. Outgrowth and branching phenotypes upon overexpression of mouse Fmn2 in wild-type embryos

Representative micrographs of motor neurons labelled by *Tg(mnx1:GFP)* in 24 hpf old *fmn2b*$^{+/+}$ embryos injected with **A)** mFmn2 mRNA and **B)** mFmn2-I1226A mRNA. **C)**

699 Quantification of branch density (number of branches per fascicle normalized to the
700 fascicle length) along the fascicle extended by motor neurons per myotome
701 hemisegment in *fmn2b*$^{+/+}$ embryos injected with mFmn2 mRNA (0.2728 ± 0.0217 $^{\mu m-1}$;
702 n=40 hemisegments) and mFmn2-I1226A mRNA (0.1617 ± 0.007 $^{\mu m-1}$; n=40
703 hemisegments). **D)** Quantification of fascicle length extended by motor neurons per
704 myotome hemisegment in *fmn2b*$^{+/+}$ embryos injected with mFmn2 mRNA (73.7 ± 1.86
705 µm; n=40 hemisegments) and mFmn2-I1226A mRNA (68.3 ± 1.603 µm; n=40
706 hemisegments). Representative micrographs of motor neurons labelled by
707 *Tg(mnx1:GFP)* in 60 hpf old *fmn2b*$^{+/+}$ embryos injected with **E)** mFmn2 mRNA and **F)**
708 mFmn2-I1226A mRNA. **G)** Quantification of branch density (number of branches per
709 fascicle normalized to the fascicle length) along the fascicle extended by motor
710 neurons per myotome hemisegment in 60 hpf *fmn2b*$^{+/+}$ embryos injected with mFmn2
711 mRNA (0.599 ± 0.027 $^{\mu m-1}$; n=28 hemisegments) and mFmn2-I1226A mRNA (0.3481
712 ± 0.02 $^{\mu m-1}$; n=28 hemisegments). **H)** Quantification of fascicle length extended by
713 motor neurons per myotome hemisegment in 60 hpf *fmn2b*$^{+/+}$ embryos injected with
714 mFmn2 mRNA (150.4 ± 1.536 µm; n=28 hemisegments) and mFmn2-I1226A mRNA
715 (145 ± 2.18 µm; n=28 hemisegments). (**** p-value <0.0001; * p-value = 0.0175; ns -
716 not significant; Kruskal Wallis test followed by Dunn's post-hoc analysis) Scale bar is
717 equivalent to 20 µm.

718

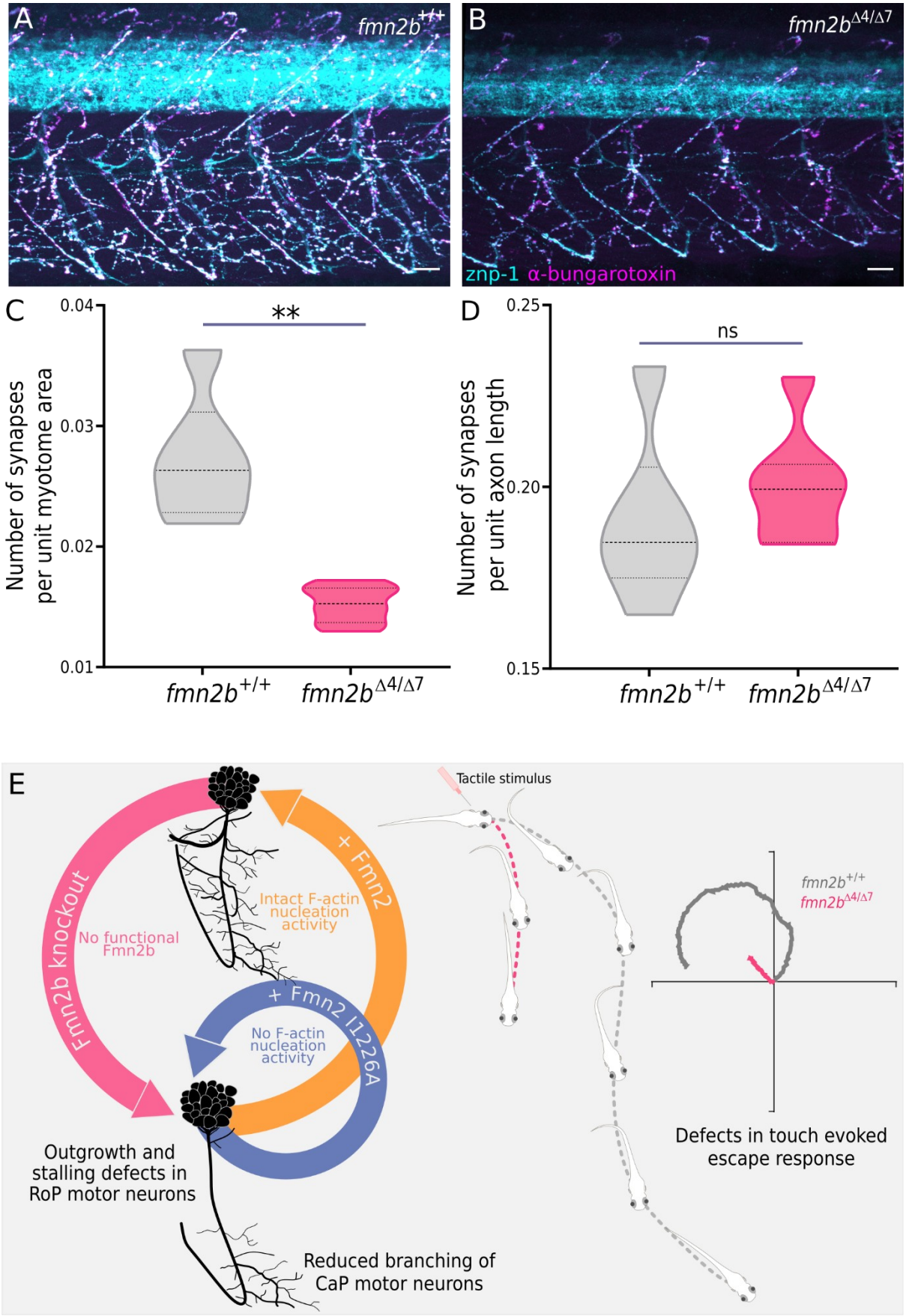

Figure 7. Synapse coverage in *fmn2b* mutants

721 Representative micrographs of 60 hpf **A)** *fmn2b*$^{+/+}$ (n=6) **B)** *fmn2b*$^{\Delta 4/\Delta 7}$ embryos (n=7)
722 co-stained with znp-1 antibody and α-bungarotoxin. Quantification of colocalization of
723 znp-1 and α-bungarotoxin in NMJ structures of 60 hpf embryos. **C)** Number of
724 synapses per unit myotome area in *fmn2b*$^{+/+}$ (0.0272 ±0.002; n=6) and *fmn2b*$^{\Delta 4/\Delta 7}$
725 embryos (0.01521 ±0.0005; n=7, **p-value=0.0012). **D)** Number of synapses per unit
726 axon length in *fmn2b*$^{+/+}$ (0.1903± 0.009; n=6) and *fmn2b*$^{\Delta 4/\Delta 7}$ embryos (0.2001± 0.005;
727 n=7). (ns- not significant; Mann Whitney U test) Scale bar is equivalent to 20 μm. **E)**
728 Depletion of Fmn2b causes outgrowth and branching defects in motor neurons in
729 zebrafish larvae causing defects in motor behaviours. The outgrowth and branching
730 defects in *fmn2b* mutants can be rescued by expression of full-length mouse Fmn2 in
731 the mutants highlighting the requirement and conserved function of Fmn2 in
732 development of motor neurons *in vivo*. The inability of mFmn2-I1226A to rescue the
733 defects in *fmn2b* mutants underscores the requirement of the F-actin nucleation
734 activity of Fmn2 in outgrowth and branching of motor neurons. The blue and orange
735 curved arrows indicate the rescue experiments with full length mFmn2 and nucleation
736 dead mFmn2-I1226A in the *fmn2b* mutant background respectively. The grey and pink
737 traces indicate the trajectories of wildtype and *fmn2b* mutant embryos respectively in
738 response to tactile stimulus. The schematic is not drawn to scale.

739 **REFERENCES**

740 Agís-Balboa RC et al. (2017) Formin 2 links neuropsychiatric phenotypes at young
741 age to an increased risk for dementia. EMBO J 36:2815–2828.

742 Ahuja R, Pinyol R, Reichenbach N, Custer L, Klingensmith J, Kessels MM, Qualmann
743 B (2007) Cordon-Bleu Is an Actin Nucleation Factor and Controls Neuronal
744 Morphology. Cell 131:337–350.

745 Armijo-Weingart L, Gallo G (2017) It takes a village to raise a branch: Cellular
746 mechanisms of the initiation of axon collateral branches. Mol Cell Neurosci 84:36–
747 47.

748 Atkins M, Gasmi L, Bercier V, Revenu C, Del Bene F, Hazan J, Fassier C (2019)
749 FIGNL1 associates with KIF1Bβ and BICD1 to restrict dynein transport velocity
750 during axon navigation. J Cell Biol 218:3290–3306.

751 Bagnall MW, McLean DL (2014) Modular Organization of Axial Microcircuits in
752 Zebrafish. Science (80-) 343:197–200.

753 Balasanyan V, Watanabe K, Dempsey WP, Lewis TL, Trinh LA, Arnold DB (2017)
754 Structure and Function of an Actin-Based Filter in the Proximal Axon. Cell Rep
755 21:2696–2705.

756 Beattie CE, Hatta K, Halpern ME, Liu H, Eisen JS, Kimmel CB (1997) Temporal
757 separation in the specification of primary and secondary motoneurons in
758 zebrafish. Dev Biol 187:171–182.

759 Bello-Rojas S, Istrate AE, Kishore S, McLean DL (2019) Central and peripheral
760 innervation patterns of defined axial motor units in larval zebrafish. J Comp Neurol
761 527:2557–2572.

762 Bernhardt RR, Chitnis AB, Lindamer L, Kuwada JY (1990) Identification of spinal
763 neurons in the embryonic and larval zebrafish. J Comp Neurol 302:603–616.

764 Bresciani E, Broadbridge E, Liu PP (2018) An efficient dissociation protocol for
765 generation of single cell suspension from zebrafish embryos and larvae.
766 MethodsX 5:1287–1290.

767 Brustein E, Saint-Amant L, Buss RR, Chong M, McDearmid JR, Drapeau P (2003)
768 Steps during the development of the zebrafish locomotor network. J Physiol Paris
769 97:77–86.

770 Carrington B, Varshney GK, Burgess SM, Sood R (2015) CRISPR-STAT: An easy and
771 reliable PCR-based method to evaluate target-specific sgRNA activity. Nucleic
772 Acids Res 43:e157.

773 Chia PH, Chen B, Li P, Rosen MK, Shen K (2014) Local F-actin network links synapse
774 formation and axon branching. Cell 156:208–220.

775 Coles CH, Bradke F (2015) Coordinating Neuronal Actin-Microtubule Dynamics. Curr
776 Biol 25:R677–R691.

777 Colombo A, Palma K, Armijo L, Mione M, Signore IA, Morales C, Guerrero N, Meynard
778 MM, Pérez R, Suazo J, Marcelain K, Briones L, Härtel S, Wilson SW, Concha ML
779 (2013) Daam1a mediates asymmetric habenular morphogenesis by regulating
780 dendritic and axonal outgrowth. Dev 140:3997–4007.

781 Das R, Bhattacharjee S, Letcher JM, Harris JM, Nanda S, Foldi I, Lottes EN, Bobo
782 HM, Grantier BD, Mihály J, Ascoli GA, Cox DN (2021) Formin3 directs dendritic
783 architecture via microtubule regulation and is required for somatosensory
784 nociceptive behavior. Development.

785 Dent EW, Gupton SL, Gertler FB (2011) The growth cone cytoskeleton in Axon

786 outgrowth and guidance. Cold Spring Harb Perspect Biol 3:1–39.

787 Dickson BJ (2002) Molecular mechanisms of axon guidance. Science (80-) 298:1959–
788 1964.

789 Drapeau P, Saint-Amant L, Buss RR, Chong M, McDearmid JR, Brustein E (2002)
790 Development of the locomotor network in zebrafish. Prog Neurobiol 68:85–111.

791 Eisen JS, Myers PZ, Westerfield M (1986) Pathway selection by growth cones of
792 identified motoneurones in live zebra fish embryos. Nature 320:269–271.

793 Fassier C, Fréal A, Gasmi L, Delphin C, Ten Martin D, De Gois S, Tambalo M, Bosc
794 C, Mailly P, Revenu C, Peris L, Bolte S, Schneider-Maunoury S, Houart C,
795 Nothias F, Larcher J-C, Andrieux A, Hazan J (2018) Motor axon navigation relies
796 on Fidgetin-like 1-driven microtubule plus end dynamics. J Cell Biol 217:1719–
797 1738.

798 Flanagan-Steet H, Fox MA, Meyer D, Sanes JR (2005) Neuromuscular synapses can
799 form in vivo by incorporation of initially aneural postsynaptic specializations.
800 Development 132:4471–4481.

801 Flynn KC, Bradke F (2020) Role of the cytoskeleton and membrane trafficking in axon–
802 dendrite morphogenesis. In: Cellular Migration and Formation of Axons and
803 Dendrites, pp 21–56. Elsevier.

804 Gallo G (2011) The cytoskeletal and signaling mechanisms of axon collateral
805 branching. Dev Neurobiol 71:201–220.

806 Gallo G (2016) Coordination of the axonal cytoskeleton during the emergence of axon
807 collateral branches. Neural Regen Res 11:709–711.

808 Ghate K, Mutalik SP, Sthanam LK, Sen S, Ghose A (2020) Fmn2 Regulates Growth

809 Cone Motility by Mediating a Molecular Clutch to Generate Traction Forces.
810 Neuroscience 448:160–171.

811 González-Fraga J, Dipp-Alvarez V, Bardullas U (2019) Quantification of Spontaneous
812 Tail Movement in Zebrafish Embryos Using a Novel Open-Source MATLAB
813 Application. Zebrafish 16:214–216.

814 Goode BL, Eck MJ (2007) Mechanism and Function of Formins in the Control of Actin
815 Assembly. Annu Rev Biochem 76:593–627.

816 Gordon-Weeks PR, Fournier AE (2014) Neuronal cytoskeleton in synaptic plasticity
817 and regeneration. J Neurochem 129:206–212.

818 Gorukmez O, Gorukmez O, Ekici A (2020) A Novel Nonsense FMN2 Mutation in
819 Nonsyndromic Autosomal Recessive Intellectual Disability Syndrome. Fetal
820 Pediatr Pathol.

821 Hale ME, Ritter D a., Fetcho JR (2001) A confocal study of spinal interneurons in living
822 larval zebrafish. J Comp Neurol 437:1–16.

823 Hu J, Bai X, Bowen JR, Dolat L, Korobova F, Yu W, Baas PW, Svitkina T, Gallo G,
824 Spiliotis ET (2012) Septin-driven coordination of actin and microtubule remodeling
825 regulates the collateral branching of axons. Curr Biol 22:1109–1115.

826 Kessels MM, Schwintzer L, Schlobinski D, Qualmann B (2011) Controlling actin
827 cytoskeletal organization and dynamics during neuronal morphogenesis. Eur J
828 Cell Biol 90:926–933.

829 Ketschek A, Gallo G (2010) Nerve Growth Factor Induces Axonal Filopodia through
830 Localized Microdomains of Phosphoinositide 3-Kinase Activity That Drive the
831 Formation of Cytoskeletal Precursors to Filopodia. J Neurosci 30:12185–12197.

832 Ketschek A, Jones S, Spillane M, Korobova F, Svitkina T, Gallo G (2015) Nerve growth
833 factor promotes reorganization of the axonal microtubule array at sites of axon
834 collateral branching. Dev Neurobiol 75:1441–1461.

835 Ketschek A, Spillane M, Dun XP, Hardy H, Chilton J, Gallo G (2016) Drebrin
836 coordinates the actin and microtubule cytoskeleton during the initiation of axon
837 collateral branches. Dev Neurobiol 76:1092–1110.

838 Kimmel CB, Ballard WW, Kimmel SR, Ullmann B, Schilling TF (1995) Stages of
839 embryonic development of the zebrafish. Dev Dyn 203:253–310.

840 Kundu T, Das SS, Kumar DS, Sewatkar LK, Ghose A (2020) Antagonistic activities of
841 Fmn2 and ADF regulate axonal F-actin patch dynamics and the initiation of
842 collateral branching. bioRxiv:2020.11.16.384099.

843 Kundu T, Dutta P, Nagar D, Maiti S, Ghose A (2021) Coupling of dynamic microtubules
844 to F-actin by Fmn2 regulates chemotaxis of neuronal growth cones. J Cell Sci.

845 Kuwada JY (1993) Pathway selection by growth cones in the zebrafish central nervous
846 system. Perspect Dev Neurobiol 1:195–203.

847 LaFave MC, Varshney GK, Vemulapalli M, Mullikin JC, Burgess SM (2014) A Defined
848 Zebrafish Line for High-Throughput Genetics and Genomics: NHGRI-1. Genetics
849 198:167–170.

850 Langebeck-Jensen K, Shahar OD, Schuman EM, Langer JD, Ryu S (2019) Larval
851 Zebrafish Proteome Regulation in Response to an Environmental Challenge.
852 Proteomics 19:1900028.

853 Law R et al. (2014) Biallelic truncating mutations in FMN2, encoding the actin-
854 regulatory protein formin 2, cause nonsyndromic autosomal-recessive intellectual
855 disability. Am J Hum Genet 95:721–728.

856 Leader B, Leder P (2000) Formin-2, a novel formin homology protein of the cappuccino
857 subfamily, is highly expressed in the developing and adult central nervous system.

858 Lewis TL, Courchet J, Polleux F (2013) Cellular and molecular mechanisms underlying
859 axon formation, growth, and branching. J Cell Biol 202:837–848.

860 Lian G, Dettenhofer M, Lu J, Downing M, Chenn A, Wong T, Sheen V (2016) Filamin
861 A- and formin 2-dependent endocytosis regulates proliferation via the canonical
862 wnt pathway. Dev 143:4509–4520.

863 Liu LYM, Lin MH, Lai ZY, Jiang JP, Huang YC, Jao LE, Chuang YJ (2016) Motor
864 neuron-derived Thsd7a is essential for zebrafish vascular development via the
865 Notch-dll4 signaling pathway. J Biomed Sci 23:1–11.

866 Lowery LA, Van Vactor D (2009) The trip of the tip: understanding the growth cone
867 machinery. Nat Rev Mol Cell Biol 10:332–343.

868 Marco EJ, Aitken AB, Nair VP, da Gente G, Gerdes MR, Bologlu L, Thomas S, Sherr
869 EH (2018) Burden of de novo mutations and inherited rare single nucleotide
870 variants in children with sensory processing dysfunction. BMC Med Genomics
871 11:50.

872 Matusek T, Gombos R, Szécsényi A, Sánchez-Soriano N, Czibula Á, Pataki C, Gedai
873 A, Prokop A, Raskó I, Mihály J (2008) Formin Proteins of the DAAM Subfamily
874 Play a Role during Axon Growth. J Neurosci 28:13310 LP – 13319.

875 McLean DL, Fetcho JR (2008) Using imaging and genetics in zebrafish to study
876 developing spinal circuits in vivo. Dev Neurobiol 68:817–834.

877 Melançon E, Liu DWC, Westerfield M, Eisen JS (1997) Pathfinding by identified
878 zebrafish motoneurons in the absence of muscle pioneers. J Neurosci 17:7796–
879 7804.

880 Menelaou E, Svoboda KR (2009) Secondary motoneurons in juvenile and adult
881 zebrafish: Axonal pathfinding errors caused by embryonic nicotine exposure. J
882 Comp Neurol 512:305–322.

883 Menon S, Gupton S (2018) Recent advances in branching mechanisms underlying
884 neuronal morphogenesis .

885 Montaville P, Jégou A, Pernier J, Compper C, Guichard B, Mogessie B, Schuh M,
886 Romet-Lemonne G, Carlier MF (2014) Spire and Formin 2 Synergize and
887 Antagonize in Regulating Actin Assembly in Meiosis by a Ping-Pong Mechanism.
888 PLoS Biol 12.

889 Montaville P, Kühn S, Compper C, Carlier MF (2016) Role of the C-terminal extension
890 of formin 2 in its activation by spire protein and processive assembly of actin
891 filaments. J Biol Chem 291:3302–3318.

892 Morello G, Guarnaccia M, Spampinato AG, La Cognata V, D'Agata V, Cavallaro S
893 (2018) Copy Number Variations in Amyotrophic Lateral Sclerosis: Piecing the
894 Mosaic Tiles Together through a Systems Biology Approach. Mol Neurobiol
895 55:1299–1322.

896 Moreno-Mateos MA, Vejnar CE, Beaudoin J-D, Fernandez JP, Mis EK, Khokha MK,
897 Giraldez AJ (2015) CRISPRscan: designing highly efficient sgRNAs for CRISPR-
898 Cas9 targeting in vivo. Nat Methods 2015 1210 12:982–988.

899 Myers PZ, Eisen JS, Westerfield M (1986) Development and Axonal Outgrowth of
900 Identified Motoneurons in the Zebrafish.

901 Nagar D, James TK, Mishra R, Guha S, Burgess SM, Ghose A (2021) The Formin
902 Fmn2b Is Required for the Development of an Excitatory Interneuron Module in
903 the Zebrafish Acoustic Startle Circuit. eNeuro 8:ENEURO.0329-20.2021.

904 Nithianandam V, Chien C-T (2018) Actin blobs prefigure dendrite branching sites. J
905 Cell Biol 217:3731–3746.

906 Pamphlett R, Morahan JM, Luquin N, Yu B (2011) Looking for differences in copy
907 number between blood and brain in sporadic amyotrophic lateral sclerosis.
908 Muscle Nerve 44:492–498.

909 Perrone MD, Rocca MS, Bruno I, Faletra F, Pecile V, Gasparini P (2012) De novo 911
910 Kb interstitial deletion on chromosome 1q43 in a boy with mental retardation and
911 short stature. Eur J Med Genet 55:117–119.

912 Pike SH, Melancon EF, Eisen JS (1992) Pathfinding by zebrafish motoneurons in the
913 absence of normal pioneer axons. Development 114:825–831.

914 Prokop A, Sánchez-Soriano N, Gonçalves-Pimentel C, Molnár I, Kalmár T, Mihály J
915 (2011) DAAM family members leading a novel path into formin research. Commun
916 Integr Biol 4:538–542.

917 Quinlan ME, Hilgert S, Bedrossian A, Mullins RD, Kerkhoff E (2007) Regulatory
918 interactions between two actin nucleators, Spire and Cappuccino. J Cell Biol
919 179:117–128.

920 Roth-Johnson EA, Vizcarra CL, Bois JS, Quinlan ME (2014) Interaction between
921 microtubules and the drosophila formin cappuccino and its effect on actin
922 assembly. J Biol Chem 289:4395–4404.

923 Sahasrabudhe A, Ghate K, Mutalik S, Jacob A, Ghose A (2016) Formin 2 regulates
924 the stabilization of filopodial tip adhesions in growth cones and affects neuronal
925 outgrowth and pathfinding in vivo. Dev 143:449–460.

926 Saint-Amant L, Drapeau P (1998) Time course of the development of motor behaviors
927 in the zebrafish embryo. J Neurobiol 37:622–632.

928 Schymick JC, Scholz SW, Fung H-C, Britton A, Arepalli S, Gibbs JR, Lombardo F,
929 Matarin M, Kasperaviciute D, Hernandez DG, Crews C, Bruijn L, Rothstein J,
930 Mora G, Restagno G, Chiò A, Singleton A, Hardy J, Traynor BJ (2007) Genome-
931 wide genotyping in amyotrophic lateral sclerosis and neurologically normal
932 controls: first stage analysis and public release of data. Lancet Neurol 6:322–328.

933 Spillane M, Gallo G (2014) Involvement of Rho-family GTPases in axon branching.
934 Small GTPases 5.

935 Spillane M, Ketschek A, Jones SL, Korobova F, Marsick B, Lanier L, Svitkina T, Gallo
936 G (2011) The actin nucleating Arp2/3 complex contributes to the formation of
937 axonal filopodia and branches through the regulation of actin patch precursors to
938 filopodia. Dev Neurobiol 71:747–758.

939 Stifani N (2014) Motor neurons and the generation of spinal motor neuron diversity.
940 Front Cell Neurosci 8:293.

941 Varshney GK, Carrington B, Pei W, Bishop K, Chen Z, Fan C, Xu L, Jones M, LaFave
942 MC, Ledin J, Sood R, Burgess SM (2016) A high-throughput functional genomics
943 workflow based on CRISPR/Cas9-mediated targeted mutagenesis in zebrafish.
944 Nat Protoc 11:2357–2375.

945 Varshney GK, Pei W, Lafave MC, Idol J, Xu L, Gallardo V, Carrington B, Bishop K,
946 Jones M, Li M, Harper U, Huang SC, Prakash A, Chen W, Sood R, Ledin J,
947 Burgess SM (2015) High-throughput gene targeting and phenotyping in zebrafish
948 using CRISPR/Cas9. Genome Res 25:1030–1042.

949 Westerfield M, McMurray J V., Eisen JS (1986) Identified motoneurons and their
950 innervation of axial muscles in the zebrafish. J Neurosci 6:2267–2277.

951 Yoo H, Roth-Johnson EA, Bor B, Quinlan ME (2015) Drosophila Cappuccino alleles

952 provide insight into formin mechanism and role in oogenesis. Mol Biol Cell
953 26:1875–1886.

ACKNOWLEDGEMENTS

The authors thank Dr. N. K. Subhedar (IISER Pune) for critical inputs on the manuscript. The authors acknowledge the IISER Pune Microscopy Facility, the National Facility for Gene Function in Health and Disease (NFGFHD) at IISER Pune and the zebrafish facility at NHGRI Zebrafish Core, NIH for access to equipment and infrastructure.

FUNDING

The study was supported from grants from the Council of Scientific and Industrial Research, Govt of India (37(1689)/17/EMR-II), Department of Biotechnology, Govt. of India (BT/PR26241/GET/119/244/2017) and intramural support from IISER Pune to A.G.. D.N. is supported by a fellowship from the Council of Scientific and Industrial Research, Govt of India. D.N. was awarded the Indo-U.S. GETin Internship (2018_050) (Department of Biotechnology (DBT), Government of India and Indo US Science and Technology Forum (IUSSTF)) which supported the CRISPR Cas9 mutagenesis work at NHGRI, NIH. The National Facility for Gene Function in Health and Disease (NFGFHD) at IISER Pune is supported by the Department of Biotechnology, Govt. of India (BT/INF/22/SP17358/2016). S.M.B. is supported by the Intramural Research Program of the National Human Genome Research Institute (ZIAHG200386-06).

AUTHOR INFORMATION

AFFILIATIONS

1. **Indian Institute of Science Education and Research (IISER) Pune, Dr Homi Bhabha Road, Pune 411008, INDIA**

   Dhriti Nagar and Aurnab Ghose

2. **Zebrafish Core, Translational and Functional Genomics Branch, National Human Genome Research Institute, National Institutes of Health, Bethesda, Maryland, USA**

   Blake Carrington

3. **Translational and Functional Genomics Branch, National Human Genome Research Institute (NHGRI), National Institutes of Health (NIH), Bethesda, MD, USA**

   Shawn M Burgess

CONTRIBUTION

Conceptualization: D.N. and A.G.; Investigation and formal analysis: D.N.; Methodology and resources: B.C. and S.M.B.; Writing – original draft: D.N. and A.G.; Writing – review and editing: D.N., B.C., S.M.B. and A.G; Funding Acquisition: A.G.. All authors gave final approval for publication and agreed to be held accountable for the work performed therein.

CORRESPONDING AUTHORS

Correspondence: Dr. Aurnab Ghose, Indian Institute of Science Education and Research (IISER) Pune, Dr Homi Bhabha Road, Pune 411008, INDIA.

Email: aurnab@iiserpune.ac.in

ETHICS DECLARATIONS

Ethics approval

All zebrafish husbandry and experimental protocols complied with institutional guidelines and were approved by the Institute Animal Ethics Committee (IAEC) and the Institutional Biosafety Committee (IBSC), IISER Pune or a National Human Genome Research Institute (NHGRI/NIH) Animal Care and Use Committee approved animal study protocol.

Consent for publication

All authors gave consent for publication.

Competing interests

The authors declare no competing interests.